UNIVERSITY OF BIRMINGHAM
University of Birmingham Research at Birmingham

Biodegradable gellan gum hydrogels loaded with paclitaxel for HER2+ breast cancer local therapy

Nieto, Celia; Vega, Milena A.; Rodríguez, Víctor; Esteban, Patricia Perez; Valle, Eva M. Martín del

DOI:
10.1016/j.carbpol.2022.119732

License:
Creative Commons: Attribution-NonCommercial-NoDerivs (CC BY-NC-ND)

Document Version
Publisher's PDF, also known as Version of record

Citation for published version (Harvard):
Nieto, C, Vega, MA, Rodríguez, V, Esteban, PP & Valle, EMMD 2022, 'Biodegradable gellan gum hydrogels loaded with paclitaxel for HER2+ breast cancer local therapy', *Carbohydrate Polymers*, vol. 294, 119732. https://doi.org/10.1016/j.carbpol.2022.119732

Link to publication on Research at Birmingham portal

General rights
Unless a licence is specified above, all rights (including copyright and moral rights) in this document are retained by the authors and/or the copyright holders. The express permission of the copyright holder must be obtained for any use of this material other than for purposes permitted by law.

•Users may freely distribute the URL that is used to identify this publication.
•Users may download and/or print one copy of the publication from the University of Birmingham research portal for the purpose of private study or non-commercial research.
•User may use extracts from the document in line with the concept of 'fair dealing' under the Copyright, Designs and Patents Act 1988 (?)
•Users may not further distribute the material nor use it for the purposes of commercial gain.

Where a licence is displayed above, please note the terms and conditions of the licence govern your use of this document.

When citing, please reference the published version.

Take down policy
While the University of Birmingham exercises care and attention in making items available there are rare occasions when an item has been uploaded in error or has been deemed to be commercially or otherwise sensitive.

If you believe that this is the case for this document, please contact UBIRA@lists.bham.ac.uk providing details and we will remove access to the work immediately and investigate.

Download date: 09. May. 2024

Carbohydrate Polymers 294 (2022) 119732

Contents lists available at ScienceDirect

Carbohydrate Polymers

journal homepage: www.elsevier.com/locate/carbpol

Biodegradable gellan gum hydrogels loaded with paclitaxel for HER2+ breast cancer local therapy

Celia Nieto [a], Milena A. Vega [a], Víctor Rodríguez [a], Patricia Pérez-Esteban [b], Eva M. Martín del Valle [a,*]

[a] Chemical Engineering Department, Faculty of Chemical Sciences, University of Salamanca, Salamanca 37008, Spain
[b] College of Health and Life Sciences, School of Biosciences, Aston University, Birmingham B4 7ET, UK

ARTICLE INFO

Keywords:
Gellan gum
Hydrogel
Local chemotherapy
HER2-positive breast cancer
Paclitaxel
β-Cyclodextrin
Glutathione

ABSTRACT

Hydrogels loaded with chemotherapeutics are promising tools for local tumor treatment. In this work, redox-responsive implantable hydrogels based on gellan gum were prepared as paclitaxel carriers for HER2-positive breast cancer therapy. To achieve different degrees of chemical crosslinking, hydrogels were synthesized in both acetate buffer and phosphate buffer and crosslinked with different concentrations of L-cysteine. It was shown that both, the type of buffer and the L-cysteine concentration used, conditioned the dynamic modulus, equilibrium swelling rate, porosity, and thermal stability of the hydrogels. Then, the biocompatibility of the hydrogels with the most suitable porosity for drug delivery applications was assessed. Once confirmed, these hydrogels were loaded with paclitaxel:β-cyclodextrin inclusion complexes, and they showed a glutathione-responsive controlled release of the taxane. Moreover, when tested *in vitro*, paclitaxel-loaded hydrogels exhibited great antitumor activity. Thus, they could act as excellent local tailored carriers of paclitaxel for future, post-surgical treatment of HER2-overexpressing breast tumors.

1. Introduction

Breast cancer is currently considered as one of the diseases with the highest mortality rate in woman worldwide (Tang et al., 2021), with 685,000 deaths associated with female breast cancer being reported last year alone (Sung et al., 2021). Among the different alternatives that exist for its treatment, surgical resection is the gold standard clinical strategy (Bu et al., 2019; Tang et al., 2021; Zhuang et al., 2020). Nevertheless, despite much improvement in surgical techniques, efficient inhibition of breast cancer recurrence still presents a challenge. The main reason for this is that residual tumor cells can remain in surgical margins (Askari et al., 2020; Bastiancich et al., 2017), particularly in patients who have undergone breast-conserving therapy (Qu et al., 2015).

To reduce the incidence of relapse, radiotherapy and chemotherapy are routinely administered in the clinical setting after tumor resection. However, both treatments are associated with high toxicity and severe systemic side effects (Bu et al., 2019; Tang et al., 2021). In addition, since these forms of treatment must begin in the weeks following surgery to allow the patient's health to recover, residual infiltrative cancer cells can keep proliferating in the meantime (Bastiancich et al., 2017; Bu et al., 2019; Zhuang et al., 2020). Moreover, resistance to chemotherapy may be promoted, in addition to other factors such as hypoxia or alterations in the signaling pathways of cancer cells, by the limited targetability of the anticancer drugs (Askari et al., 2020; Kibria & Hatakeyama, 2014). For these reasons, local delivery of chemotherapeutics in the tumor resection cavity is becoming increasingly desirable for breast cancer treatment (Tang et al., 2021). Compared to systemic therapies, local chemotherapy can prevent drugs from being non-specifically distributed and can avoid off-target toxicities. Moreover, local chemotherapy may eliminate the latency time of post-surgical systemic chemotherapy (Askari et al., 2020; Tang et al., 2021; Zhuang et al., 2020).

Among the different types of drug delivery systems (DDS) designed for antitumor local therapies, hydrogels are, in particular, generating greater interest, as their mechanical properties can be tailored to mimic those of the extracellular matrix (ECM) of living tissues (Askari et al., 2020). Furthermore, most of these three-dimensional hydrophilic networks are made from natural polymers; thus, they are biocompatible, biodegradable and easily modifiable, in addition to having high drug-

* Corresponding author.
E-mail address: emvalle@usal.es (E.M. Martín del Valle).

https://doi.org/10.1016/j.carbpol.2022.119732
Received 3 February 2022; Received in revised form 30 May 2022; Accepted 9 June 2022
Available online 15 June 2022
0144-8617/© 2022 The Authors. Published by Elsevier Ltd. This is an open access article under the CC BY-NC-ND license (http://creativecommons.org/licenses/by-nc-nd/4.0/).

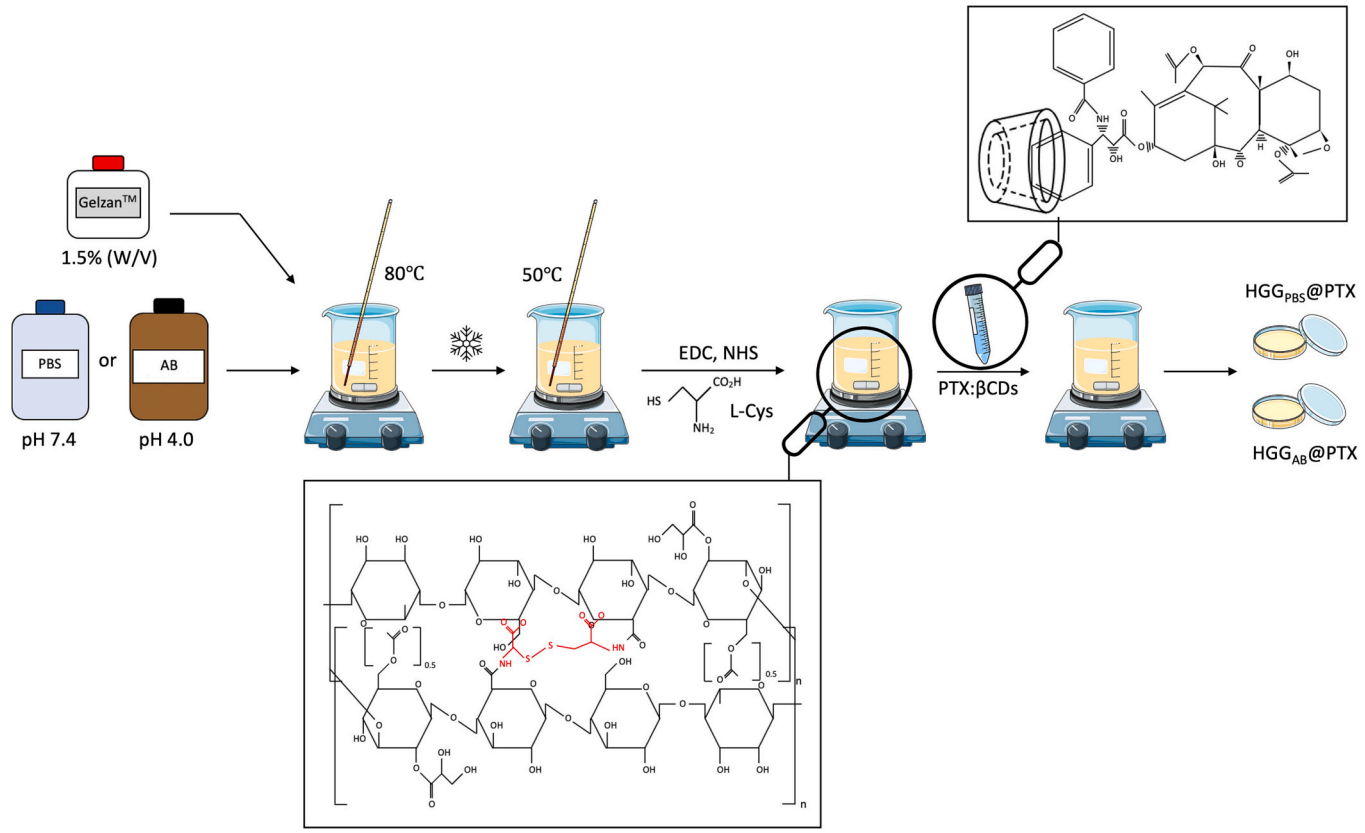

Scheme 1. Schematic representation of the preparation of the HGG patches, chemically crosslinked with different concentrations of L-Cys and loaded with PTX:β CD complexes.

loading capacities (Abasalizadeh et al., 2020; Darge et al., 2019; Misra & Acharya, 2021; Sharma & Tiwari, 2020). Among the most common natural polymers, gellan gum (GG) is gaining attractiveness for biomedical purposes, as it is stable and has appropriate mechanical properties, acid and heat resistance and inotropic sensitivity. GG is an extracellular polysaccharide, which contains repeating units of β-D-glucose, L-rhamnose, and D-glucuronic acid in a 2:1:1 M ratio (Das & Giri, 2020; Palumbo et al., 2020), that can undergo thermally reversible gelation after a coil-helix transition in the presence of mono- (K^+, Na^+) or divalent (Ca^{2+}) cations (Bacelar et al., 2016; Prajapati et al., 2013; Soleimani et al., 2021). Similarly, GG can be chemically crosslinked to maintain stable biomaterial structures for longer periods. Previous works involving this polysaccharide have been reported regarding its use for the delivery of several anticancer drugs (paclitaxel, doxorubicin, erlotinib and clioquinol, among others) to improve their solubility, intra-tumoral specificity, and drug release profile *via* hydrogels, patches and nanoconfigurations (Villareal-Otalvaro & Coburn, 2021). In the specific case of paclitaxel (PTX), GG has been employed to develop *in situ*-gelling liposome-in-gel composites containing this drug for local bladder cancer treatment, and nanohydrogels delivering the taxane along with prednisolone for prostate cancer and inflammatory carcinoma applications (D'Arrigo et al., 2014; GuhaSarkar et al., 2017). However, GG has not yet been used to fabricate PTX-loaded implantable hydrogel patches for local, stimuli-responsive treatment of HER2-positive (HER2+) breast tumors. Therefore, the main aim pursued in this work was to develop, characterize and validate *in vitro* PTX-releasing GG hydrogel patches that would be suitable for this novel application: local and redox-responsive antitumor therapy of HER2+ breast tumors.

Consequently, GG hydrogels (HGGs) were prepared in two solutions with different pH and ionic compositions (acetate buffer [AB] *vs.* phosphate buffered saline [PBS]) and were disulfide-crosslinked with different L-cysteine (L-Cys) concentrations utilizing the carbodiimide chemistry to improve their stability while achieving responsiveness to external reducing stimuli, such as the high glutathione (GSH) concentrations existing in malignant breast cells (Li et al., 2020; Pérez et al., 2014). The main aim of synthesizing HGGs in different buffers and with different L-Cys concentrations was examining how these parameters conditioned their crosslinking degree and, therefore, their dynamic modulus, equilibrium swelling rate, porosity, and thermal stability. Then, all these hydrogel properties were analyzed and, based on the results obtained, those HGGs with the most appropriate characteristics for drug delivery applications were selected to be loaded with PTX. This taxane was previously included in β-cyclodextrin (βCD) molecules to improve its limited aqueous solubility (Nieto et al., 2019; Tian et al., 2020), and the resulting complexes (PTX:βCDs) were included in the GG patches to enhance the redox-controlled release of PTX while trying to improve its bioavailability and off-target toxicity through a potential local application (Scheme 1). Antitumor activity of the HGGs loaded with the PTX:βCD complexes was evaluated *in vitro* after analyzing their biocompatibility, and the results obtained showed that they may be a promising strategy for post-surgical chemotherapy of HER2-overexpressing breast tumors with elevated GSH intracellular concentrations.

2. Materials and methods

2.1. Materials

Gelzan™ CM (G1910, average molecular weight: 1000 kg/mol; low-acyl [0.2 %]; monosaccharide composition: β-D-glucose:L-rhamnose:D-glucuronic acid [2:1:1]), β-cyclodextrin (βCD, minimum 98 %), paclitaxel (PTX, from semisynthetic, >97 %), L-cysteine (L-Cys, 97 %), lysozyme human, 1-ethyl-3-(3-dimethylaminopropyl) carbodiimide (EDC),

N-hydroxy succinimide (NHS), thiazolyl blue tetrazolium bromide (MTT), phosphate buffered saline (PBS, powder [NaCl [137 mM], KCl [2.7 mM], Na_2HPO_4 [10 mM], KH_2PO_4 [1.8 mM], pH 7.4) and L-Glutathione reduced (>98 %) were all obtained from Sigma Aldrich (St. Louis, MO, USA). Dimethyl sulfoxide (DMSO, >99 %) and Corning™ penicillin/streptomycin solution (100×: penicillin [100 UI/ml] and streptomycin [10,000 μg/ml]) were purchased from Thermo Fisher Scientific (Waltham, MA, USA). Calcein AM and propidium iodide (PI, Ready Probes™) were obtained from Invitrogen (Carlsbad, CA, USA). Potassium bromide (for IR), acetic acid glacial, citric acid anhydrous, sodium acetate anhydrous, sodium citrate, sodium chloride, tris hydrochloride and absolute pure ethanol (EtOH) were all obtained from Panreac AppliChem (Castellar del Vallès, Barcelona, Spain). Dubelcco's Modified Eagle's Medium (DMEM) and fetal bovine serum (FBS, qualified, HI) were purchased from Gibco (Gaithersburg, MD, USA). Finally, lactate dehydrogenase activity colorimetric assay kit (product code: ab102526) was obtained from Abcam (Cambridge, UK).

2.2. Synthesis of HGG patches

To prepare the HGG patches, Gelrite® (Gelzan™) was chosen among the main different commercial forms of GG because it disperses and hydrates well in deionized water (H_2O[d]) and is inert to most biological growth media additives (Prajapati et al., 2013). In this way, Gelzan™ was dissolved (1.5 % [*w/v*]) both in 80 °C AB (0.05 M, pH 4.0) and in 80 °C PBS (pH 7.4) (Matricardi et al., 2009; Oliveira et al., 2016). Once homogeneous solutions were obtained, the temperature was lowered to 50 °C. Solutions of EDC (2.9 mg/ml) and NHS (4.8 mg/ml) were later incorporated consecutively (1:50 [*v/v*]). After stirring briefly, L-Cys solutions of different concentrations (1.5, 3, and 4.5 mg/ml) were added (1:50 [v/v]) to achieve different degrees of GG chemical crosslinking (Wu et al., 2018; Yu et al., 2020). Final solutions were poured into dishes and left for gelation at room temperature overnight.

2.3. Rheology

Rheological measurements of 2-mm-thick HGGs were performed using an AR 1500 Ex rheometer (Waters Corporation, Milford, MA, USA) equipped with an aluminum parallel plate geometry (plate diameter 40 mm, gap distance 1 mm). HGG samples were prepared using 33 mm-diameter dishes as templates, carefully unmolded preventing breakage and placed on the lower plate of the rheometer. To evaluate their stiffness, dynamic oscillation-frequency tests were carried out in duplicate in the 0.01–10 Hz range at 25 °C and 37 °C by applying a $\gamma = 0.01$ constant deformation in the linear viscoelastic region. This region was preliminary assessed using stress sweep tests (Matricardi et al., 2009) (data not shown).

2.4. Swelling test

The swelling ability of the different HGGs was assessed *via* a general gravimetric method. Variations in weight were recorded over time when the HGGs were soaked in solutions of different pH and ionic strength: H_2O(d) (purified with the Economatic Wasserlab equipment [Barbatáin, Navarra, Spain]); commercial mineralized water (H_2O[c]); NaCl solution (0.015 M); tris buffer (0.05 M); citrate buffer (0.1 M); AB (0.04 M); PBS (1×); and DMEM supplemented with FBS and antibiotics. Briefly, after gelation, hydrogel disks (35 mm diameter, 8 mm height) were frozen at −80 °C, lyophilized overnight (LyoQuest lyophilizer, Telstar, Lisbon, Portugal), and weighed. Then, hydrogels were immersed in the previously mentioned solutions (50 ml), removed after different time points, wiped superficially with bibulous paper, weighed again, and introduced in the same solutions (Coutinho et al., 2010; Li et al., 2021; Morello et al., 2021). The swelling ratios at time t (Q_t) and when HGGs reached equilibrium (Q_∞) were defined according to Eqs. (1) and (2), respectively, where m_0 is the initial weight of the dried gels (g), m_t is the weight of the swelled gels after time t (g), and m_∞ is the weight of the swelled gels at the equilibrium (g) (Schott, 1992).

$$Q_t = \frac{m_t - m_0}{m_0} \tag{1}$$

$$Q_\infty = \frac{m_\infty - m_0}{m_0} \tag{2}$$

To better describe the swelling behavior of the HGGs, a swelling kinetic study was performed at the initial stage of swelling, until hydrogels reached equilibrium. For this purpose, Eqs. (1) and (2) were adjusted to a pseudo-second-order kinetic model, as described by Schott in 1992 (Supplementary Material). It was considered that homogeneous uptake of the solutions occurred throughout the hydrogel polymer networks.

2.5. Evaluation of the crosslinking density

The effective crosslinking density (d_x, mol/ml) of the six different prepared HGGs was determined according to Eq. (3):

$$d_x = \frac{1}{\vartheta M_c} \tag{3}$$

where ϑ is the specific volume of the polymer (ml/g) and M_c is the average molecular mass between crosslinkings (g/mol), which was determined by the Flory-Rehner equation (Eq. (4)):

$$M_c = \frac{\rho_p V_s V_r^{1/3}}{\left[ln(1 - V_r) + V_r + XV_r^2\right]} \tag{4}$$

where V_s is the molar volume of the solvent (ml/mol), ρ_p is the density of the polymer (g/ml), X is the parameter of interaction between the solvent and the polymer (which has a value of 0.81 ± 0.05 for aqueous solutions of GG (Safronov et al., 2019) and V_r is the polymer volume fraction calculated from Eq. (5).

$$V_r = \left[1 + \frac{\rho_p}{\rho_s}\left(\frac{M_a}{M_b}\right) + \frac{\rho_p}{\rho_s}\right] \tag{5}$$

where M_a is the swollen hydrogel weight (g), M_b is the weight of the dried hydrogel before the swelling experiment (g) and ρ_s is the density of the solvent (g/ml) (Afinjuomo et al., 2019; Sabadini et al., 2018).

2.6. Morphological analysis and porosity determination after freeze-drying

The porous structure of the different HGGs synthesized was analyzed by scanning electron microscopy (SEM) (ESEM Quanta 200 FEG, FEI, Hillsboro, OR, USA). HGG samples were freeze-dried, coated with gold and cross-sectioned. Then, samples were imaged at an accelerating voltage of 15 kV. 8 to 10 images were acquired from different areas of each sample and the average diameter of the micro- and macropores existing in the HGGs was determined *via* image analysis (ImageJ software) (Hua et al., 2016; Lee et al., 2020).

In addition, HGG porosity was measured using Archimedes' principle. Once synthesized, all hydrogel samples were freeze-dried and completely immersed in tubes filled with absolute EtOH. After 24 h, HGGs were removed from the tubes and their porosity was calculated according to Eq. (6):

$$Porosity\ (\%) = \frac{W_2 - W_{3\_} W_s}{W_1 - W_3} \times 100 \tag{6}$$

where W_1 is the weight of the tube filled with EtOH (g), W_2 is the weight of the tube filled with EtOH 24 h after immersion of the freeze-dried HGGs (g), W_3 is the weight of the tube filled with EtOH after HGG removal (g) and W_S is the weight of the freeze-dried HGGs (g) (Goodarzi et al., 2019).

2.7. Fourier transform infrared (FTIR) characterization

The chemical structure of all HGG samples, as well as that of GG, was analyzed by FTIR spectroscopy (Spectrum Two™ spectrometer, Perkin Elmer, Waltham, MA, USA) at the wavelength range of 900–4000 cm^{-1} and compared. Freeze-dried samples were ground to powder, dried at 37 °C for 3 days to remove any possible residual water, prepared with KBr pellets, and scanned.

2.8. Thermogravimetric analysis (TGA)

HGG thermal stability was analyzed by TGA (DSC Q100 calorimeter, Waters Corporation, Milford, MA, USA) and compared to that of GG alone. HGGs were freeze-dried, and all samples were later ground to powder and heated at a rate of 10 °C/min from 50 °C to 600 °C under a nitrogen atmosphere to obtain the thermogravimetric (TG) curves.

2.9. Compression test

The compressive modulus of cylinder samples (35 mm diameter, 8 mm height) of the HGGs chosen to be later loaded with the PTX:βCD complexes was determined by spherical indentation testing. Thus, a spherical indenter was employed as plunger (Fig. S1), the force-indentation curve for the samples was recorded, and the effective stiffness of the hydrogels was extracted. For this purpose, the indentation curves obtained were fitted to Hertz's contact model (Eq. (7)) (Srivastava et al., 2017).

$$F = -\frac{16E_2\sqrt{Rd^3}}{9} \tag{7}$$

where F was the force applied by the indenting bead (N), E_2 was the Young's modulus of the different HGG samples (kN/m^2), R was the diameter of the bead (6 mm) and d was the indentation depth (mm). HGG average Young's modulus was determined from the slope obtained after plotting F *vs.* $d^{3/2}$. Three parallel samples were tested to obtain an average.

2.10. Hydrogel in vitro degradation

The degradation rate of the HGGs (35 mm diameter, 8 mm height) later loaded with the PTX:βCD complexes was investigated *in vitro* through weight loss under simulated tumor extracellular pH conditions. Once weighed (m_0, g), HGGs were placed in duplicate in beakers containing lysozyme solution (1 mg/ml in PBS (pH 6.8)) and incubated for 9 days at 37 °C under gentle shaking (50 rpm). HGGs were weighed daily (m_t, g) after wiping their surface with bibulous paper, and their weight loss (m_r) was determined according to Eq. (8) (Huang et al., 2020; Lu et al., 2022; Panczyszyn et al., 2021; Xu et al., 2018):

$$m_r(\%) = \frac{m_0 - m_t}{m_0} \times 100 \tag{8}$$

2.11. Cell culture and hydrogel biocompatibility in vitro

Human HER2+ breast carcinoma BT474 cells and stromal HS5 cells were grown in DMEM supplemented with 10 % (*v*/v) FBS and 1 % (v/v) penicillin/streptomycin, and cultured in an atmosphere of 5 % CO_2 at 37 °C.

HGG biocompatibility was doubly assessed by MTT assays and live/death staining. BT474 and HS5 cells were seeded in 24-well plates (12,000 cells/ml), grown for 24 h for attachment, and cultured with HGG samples that were allowed to gel for 90 min (23.1 % [*v*/v], previously sterilized by UV radiation). Cells were incubated for 72 h and their survival rate was studied by MTT colorimetry tests. At specified times (including 24, 48 and 72 h), 110 μl MTT solution (5 mg/ml in PBS) was added to the wells, cells were incubated further for 1 h at 37 °C, and the resulting formazan salts were dissolved in DMSO (500 μl/well) (Rahnama et al., 2021). The optical density (OD) of each well was recorded using a microplate reader (EZ Microplate Reader 2000, Biochrom, Cambridge, UK) at a wavelength of 550 nm after shaking for 10 min. Cells not exposed to HGG samples were used as a blank control group, and three independent samples were included for each time interval and experimental group.

BT474 and HS5 cells were also seeded in 8-well glass-bottom slides (12,000 cells/ml), grown for 24 h and exposed or not to HGG samples (23.1 % [*v*/v], also sterilized by UV radiation) for a further 24 h. Then, 15 min before imaging the cells by confocal laser scanning microscopy (CLSM), calcein AM (1 μg/ml) and PI (5 μg/ml) were used to stain alive (green) and dead (red) cells, respectively (Huan et al., 2022). Samples (two independent ones for each experimental group) were washed with PBS solution before CLSM imaging (TCS SPS, Leica Microsystems, Wetzlar, Germany).

2.12. HGG loading with PTX:βCD complexes

To improve PTX aqueous solubility, PTX:βCD inclusion complexes were obtained following the freeze-drying method described by Alcaro et al., 2002. Briefly, PTX (1 mg) was dissolved in absolute EtOH (1.2 ml), and βCDs (1.2 mg) were dissolved in H_2O(d) (1.4 ml). Next, the βCD solution was added to the PTX solution, and the resulting hydroalcoholic solution was kept under agitation (100 rpm) for 5 h at room temperature and in the dark. Later, it was frozen at −80 °C and freeze-dried (Nieto et al., 2019). The white powder obtained was dissolved in H_2O(d), achieving a 0.185 mM PTX working concentration.

Subsequently, to load HGG patches with the PTX:βCDs prepared, hydrogel synthesis was performed as described above. PTX:βCD solutions were added while the gelation process was taking place, once the L-Cys solutions (3 mg/ml) were incorporated (Ning et al., 2020). HGGs loaded with the chemotherapeutic (HGGs@PTX) were allowed to cool in dishes or multi-well plates for their complete gelation.

2.13. PTX-release from HGGs in vitro

Once obtained, crosslinked HGGs@PTX were allowed to gel for 90 min and washed with PBS to remove the unloaded taxane before performing drug release experiments in duplicate. Next, hydrogel patches (35 mm diameter, 8 mm height) were soaked in crystallizing dishes containing slightly acidic PBS (60 ml, pH 6.8) and incubated at 37 °C at 40 rpm for 72 h. To mimic the intracellular redox potential of tumor cells, GSH was added in high concentrations (10 mM) to the release medium of some HGG samples (Pérez et al., 2014; Robby et al., 2021). At pre-determined times, 0.5 ml aliquots were taken out, and equal volumes of acidic PBS (containing or not GSH [10 mM]) were added to maintain a constant volume in the crystallizing dishes. The amount of PTX released was calculated by comparing the absorbance of the aliquots at 230 nm (UV-1800 spectrophotometer, Shimadzu Corporation, Kioto, Japan) with a previously measured calibration curve obtained from a PTX dilution series. Aliquots of the release media of non PTX-loaded HGGs were used as a blank. Cumulative PTX release (%) from the different HGGs samples was determined according to Eq. (9) and plotted against time (Fang et al., 2021; Rezk et al., 2019; Vu et al., 2022).

$$PTX\ released\ (\%) = \frac{Total\ PTX\ released}{Total\ PTX\ in\ HGGs} \times 100 \tag{9}$$

Moreover, PTX release kinetics were studied through four different mathematical models, *i.e.*, zero-order, first-order, Korsmeyer-Peppas and Higuchi models. A description of the method is reported in the Supplementary Material.

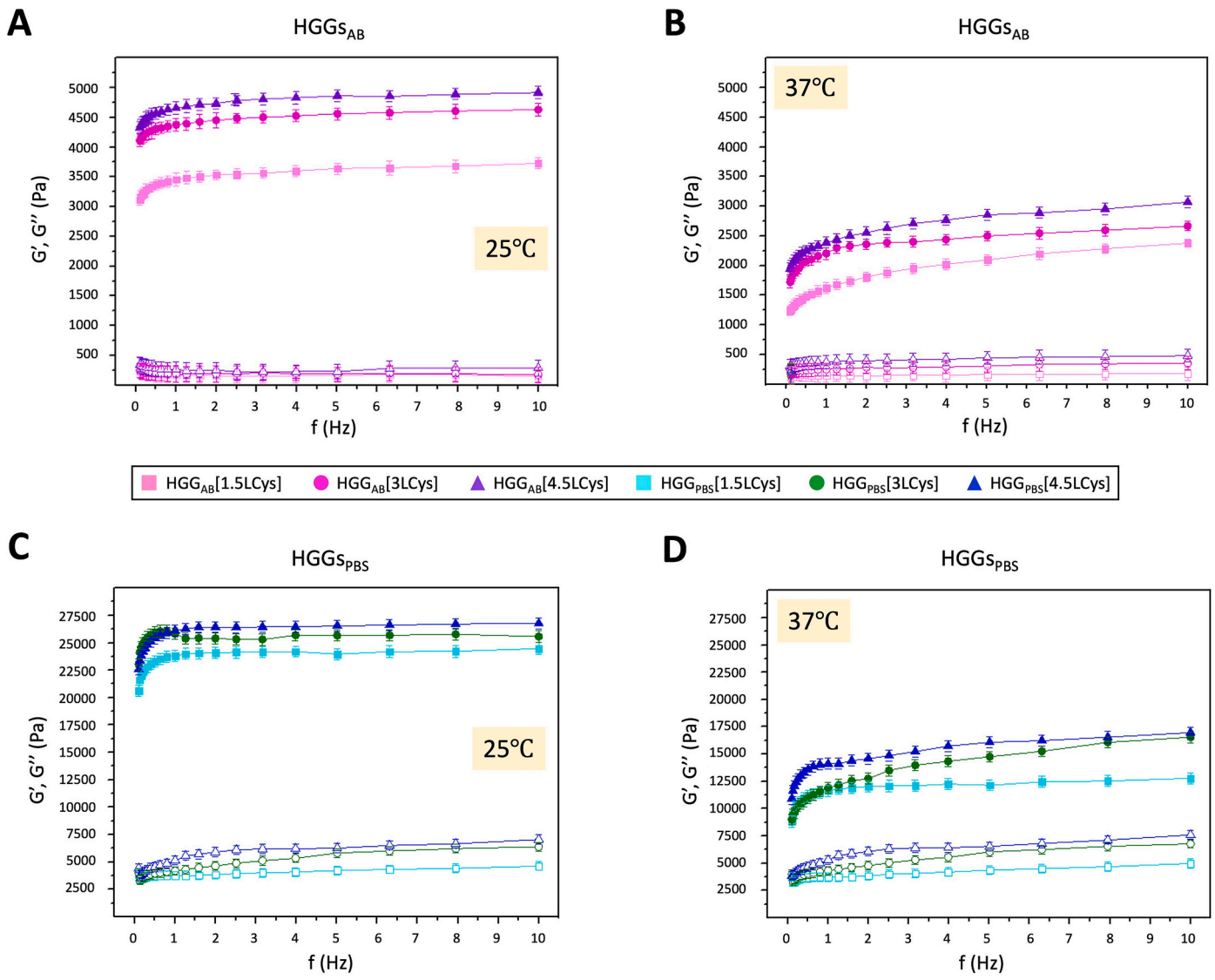

Fig. 1. Frequency sweeps of the different synthesized HGGs$_{AB}$ and HGGs$_{PBS}$ performed at 25 °C (**A**–**C**) and 37 °C (**B**–**D**). Filled symbols represent G′ values, while empty symbols are G″ values. The concentration of L-Cys used to crosslink the different hydrogels is indicated between brackets (in mg/ml).

2.14. Antitumor activity of HGGs@PTX in vitro

HGG@PTX antitumor activity was analyzed *in vitro* on two different human HER2-overexpressing breast carcinoma cell lines: BT474 and SKBR3 (Nieto et al., 2019).

Cells were cultured as previously indicated, and MTT assays and live/death staining were conducted following the same protocols as before to doubly assess crosslinked HGG@PTX cytotoxicity. Nevertheless, this time, BT474 and SKBR3 cells were exposed to HGGs (23.1 % [*v*/v]), HGGs@PTX (23.1 % [v/v]) and PTX:βCDs (in an equivalent concentration to that loaded to the HGGs (30.8 μM)). Besides, live/death staining was performed 48 and 72 h after cell exposure to the different treatment conditions. Again, cells not exposed to HGG samples served as a blank control group in both assays.

In addition, lactate dehydrogenase (LDH) leakage assays were carried out according to LDH activity detection kit manufacturer's instructions to analyze BT474 and SKBR3 membrane damage after treatment with the HGGs[3LCys]@PTX for 48 h. Group distributions and PTX:βCDs and HGG[3LCys]@PTX concentrations similar to those in the MTT assays were employed. The absorbance of the LDH expression was assessed at 450 nm using a microplate reader.

2.15. Statistical analysis

All data were reported as mean ± standard deviation (SD). Specific comparison between groups was carried out with unpaired Student's *t*-tests, while one-way ANOVA was used for multiple-group comparison. *p*-values <0.05 were considered to be statistically significant. When statistically significant differences were found when performing one-way ANOVA, Tukey test was carried out as *post-hoc* analysis.

3. Results and discussion

3.1. Preparation of HGGs with different degrees of chemical crosslinking

One of the characteristics of GG that has led to its increased use for biomedical purposes is its ionotropic sensitivity (Das & Giri, 2020; Palumbo et al., 2020). In this way, obtaining HGGs is possible because, when mono- or divalent cations are present in a solution, GG can undergo thermally reversible gelation after transition from a coiled form at high temperature (>80 °C) to a double-helix structure when cooled (Bacelar et al., 2016; Prajapati et al., 2013). Thus, HGG consistency can be modified, apart from altering the concentration of the gum, by adding different ions to GG solutions (Das & Giri, 2020; Palumbo et al., 2020).

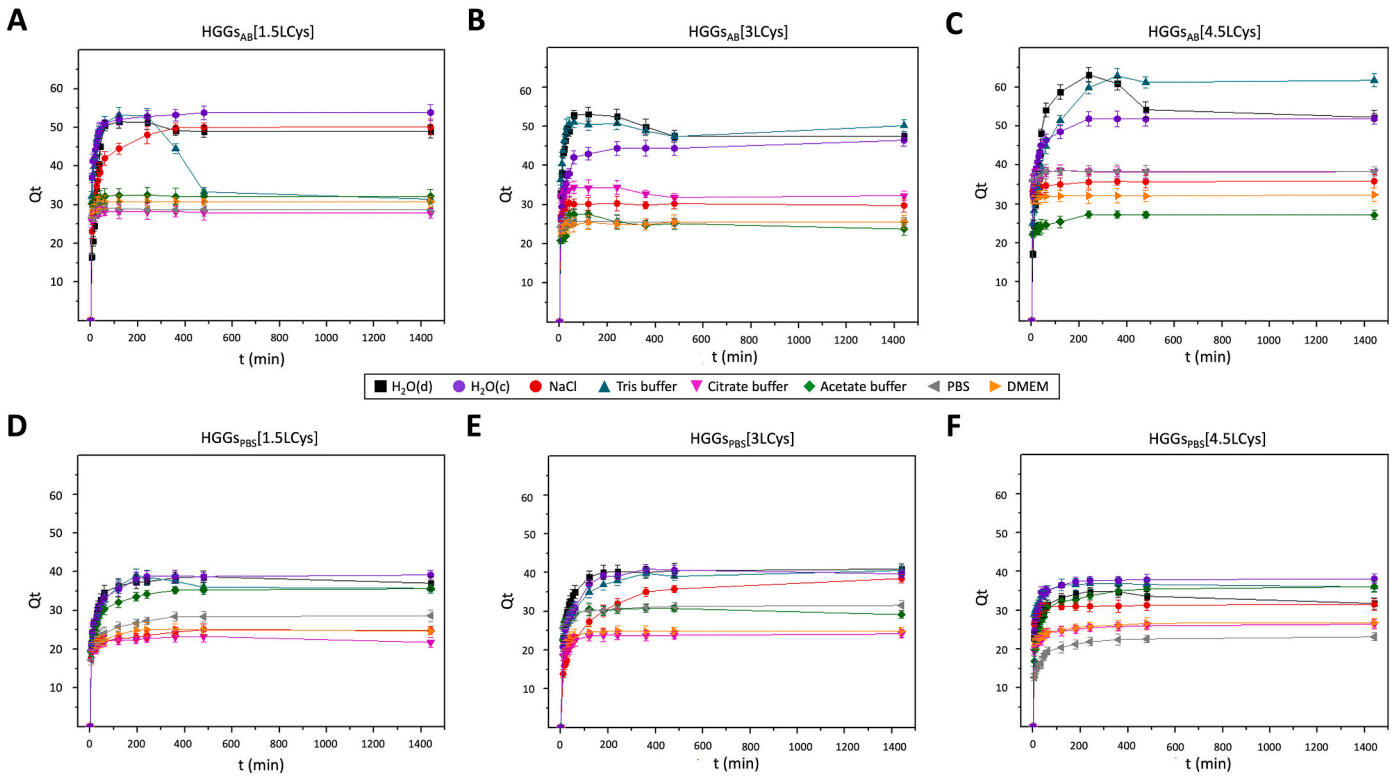

Fig. 2. Swelling kinetics of the different HGGs$_{AB}$ (**A**–**C**) and HGGs$_{PBS}$ (**D**–**F**) as a function of the swelling time when soaked in solutions with different pH and ionic strength at 25 °C.

For this reason, as indicated in Scheme 1, two buffers of different ionic composition and pH (AB *vs.* PBS) were used in this work to synthesize HGGs with the aim of analyzing how they conditioned the physicochemical properties of the hydrogels obtained (HGGs$_{AB}$ *vs.* HGGs$_{PBS}$ respectively) (Matricardi et al., 2009; Oliveira et al., 2016). In addition, to enhance their stability and make them redox-responsive, HGGs were chemically crosslinked with L-Cys (Du et al., 2012), which was employed in three different concentrations (1.5, 3, and 4.5 mg/ml) to later choose the most suitable hydrogels to act as PTX delivery systems. EDC chemistry was used to carry out the crosslinking because, unlike other compounds frequently used to prepare chemical hydrogels, EDC and NHS are not cytotoxic in concentrations below 0.5 M (Hua et al., 2016; Panczyszyn et al., 2021). In addition, these compounds have already been used in the literature to crosslink hydrogels made up of other polymers (Goodarzi et al., 2019; Pacelli et al., 2018; Výborný et al., 2019), and the N-hydroxysuccinimidyl ester coupling chemistry is one of the few conjugation strategies utilized in the development of FDA-approved protein conjugates (Kang et al., 2021; Pelegri-O'Day et al., 2014).

3.2. Rheological properties of the different HGGs

Once obtained, the viscoelastic properties of the six different synthesized types of HGG were determined employing dynamic oscillatory frequency sweep assays and compared. Mechanical spectra recorded both at 25 °C and 37 °C can be found in Fig. 1.

As can be observed in Fig. 1, the frequency sweeps obtained indicated that all samples had characteristic gel behavior, since the storage modulus (G′) was at least 10 times higher than the loss modulus (G″) in all cases. Moreover, both G′ and G″ were almost independent of the frequency, which is a distinctive fact of entangled gels (Matricardi et al., 2009; Richa & Choudhury, 2019). However, when comparing the spectra of the different HGGs$_{AB}$ (Fig. 1[A–B]) with those of the HGGs$_{PBS}$ (Fig. 1[C–D]), it was observed that G′ values were greater when hydrogels were prepared in PBS than in AB. In this way, HGGs$_{PBS}$ gelled faster and were more viscous than HGGs$_{AB}$. This result was logical considering that PBS contains K^+ cations and higher concentrations of Na^+ cations (>10 times greater) than AB (Table S1) and, therefore, that it could contribute to achieving greater degree of GG crosslinking.

As expected, when the L-Cys content of both HGGs$_{AB}$ and HGGs$_{PBS}$ was higher, G′ values increased due to the existence of more chemical crosslinkings and the consequent formation of stronger 3D networks. This trend could be also seen when increasing the measurement temperature from 25 °C to 37 °C, although this increase in temperature resulted in diminished G′ values, which were 40–60 % lower than those recorded at 25 °C (Matricardi et al., 2009). Hence, this reduction in the elastic modulus suggested that HGG equilibrium constants were thermal sensitive, and that this sensitivity could be related to the initial degree of crosslinking of the HGGs, since G′ reduction was less noticeable when hydrogels were disulfide-crosslinked with higher concentrations of L-Cys and when they were synthesized in PBS instead of in AB (Roberts et al., 2007).

3.3. Swelling behavior of the different HGGs as a function of the medium pH and ionic strength

Since the rate and degree of swelling of hydrogels are the most important parameters when controlling the release of the drugs with which they may be loaded (Ganji et al., 2010), the swelling kinetics of all HGGs prepared were analyzed as a function of the medium pH and ionic strength (μ). For this purpose, HGG samples were soaked in H$_2$O(d) and H$_2$O(c) to determine whether their different ionic composition conditioned hydrogel swelling capacity. Likewise, HGGs were soaked in NaCl solutions, PBS and supplemented DMEM because these media with different ionic strength mimic physiological fluids. Moreover, tris buffer, citrate buffer and AB were also employed to perform swelling assays to try to determine how the medium acidity or basicity could condition HGG absorption capacity. The properties of all these media can be found

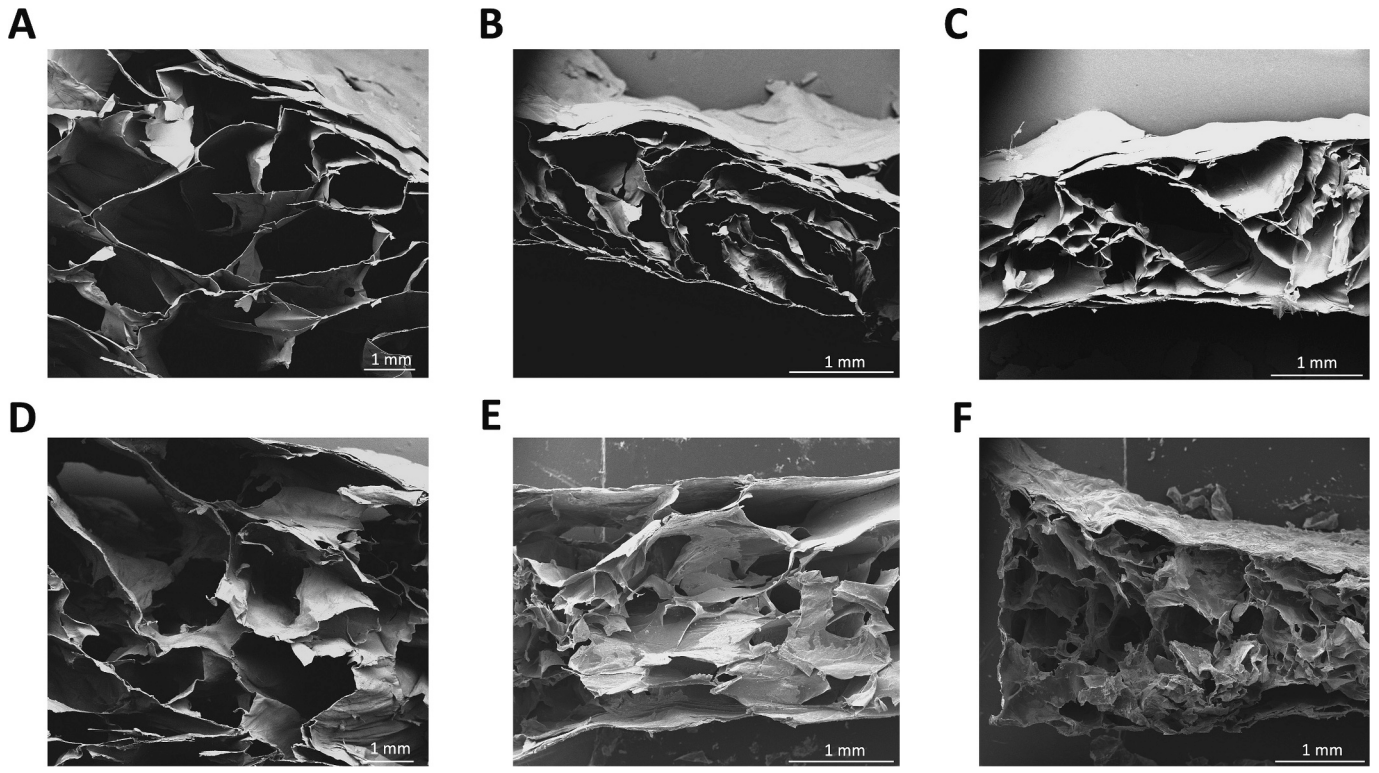

Fig. 3. Morphological analysis under SEM of (**A**) HGG_{AB}[1.5LCys], (**B**) HGG_{AB}[3LCys], (**C**) HGG_{AB}[4.5LCys], (**D**) HGG_{PBS}[1.5LCys], (**E**) HGG_{PBS}[3LCys] and (**F**) HGG_{PBS}[4.5LCys] samples.

in Table S2.

The swelling kinetics obtained for the $HGGs_{AB}$ crosslinked with different concentrations of L-Cys are shown in Fig. 2(A–C), while those of the three different $HGGs_{PBS}$ can be seen in Fig. 2(D–F).

As shown in Fig. 2, most HGG samples reached equilibrium after 240 min. Thereby, after soaking HGGs in the different media for about 4 h, there was a balance between the osmotic forces caused by the solutions when entering the hydrogel macromolecular networks and the cohesive-elastic forces exerted by the GG chains, which opposed the expansion. For this reason, the experimental data obtained up to 240 min were adjusted to a pseudo-second-order kinetic model to determine Q_∞ and K_∞ values for all $HGGs_{AB}$ and $HGGs_{PBS}$ in the different media (Panpinit et al., 2020; Schott, 1992). The values obtained for these parameters, which refer to the theoretical equilibrium swelling capacity and the swelling rate constant of the HGGs, respectively, are indicated in Table S3 and S4.

When comparing the parameters of the swelling kinetics of both types of HGGs as a function of their crosslinking degree, it was noticed that, in general, the greater crosslinking, the lower the HGG swelling capacity. This fact was in line with what was expected since by increasing L-Cys concentration during the synthesis process, it was likely that HGG pore size would be reduced, and that hydrogels would take up less volume when soaked in the different media (Coutinho et al., 2010).

In the same way, as the degree of crosslinking of the $HGGs_{AB}$ was lower than that for the $HGGs_{PBS}$, they showed greater swelling capacity and, therefore, higher Q_∞ and K_∞ values, especially in the most alkaline media: H_2O(d), H_2O(c), tris buffer and DMEM. Possibly, as described in the literature, H^+ cations could interact with GG negative charges after penetrating the hydrogel structure, causing greater aggregation of GG chains at low pH values. By contrast, in basic media, OH^- anions may accelerate the electrostatic repulsion of GG chains, causing hydrogels to experience a hydrolysis-induced swelling behavior and to have higher swelling rates than in acidic solutions (Cassanelli et al., 2018; De Souza et al., 2016; Moritaka et al., 1995; Zhou & Jin, 2020). In fact, when HGGs were soaked in H_2O(d) and, especially, in tris buffer, they started to break after 30 min, possibly because the electrostatic repulsion between the COO^- anions was too strong and hydrogels lost their network structure. In addition, as shown in Fig. 2, the less crosslinked $HGGs_{AB}$ experienced over-swelling when soaked in tris buffer, followed by a deswelling process that took place until they reached equilibrium. Probably, since these HGGs could oppose less resistance to the entry of tris buffer in their structure, this phenomenon could take place because of the difference in osmotic pressure that occurred at the initial stage of the swelling process (Li et al., 2021).

Finally, regarding the effect of the ionic strength of the media on HGG swelling behavior, another phenomenon already described in the literature could be observed: in those media with greater ionic strength (DMEM, PBS, citrate buffer, AB and NaCl solution), HGG swelling occurred in a lesser extent than in media with less ions (H_2O[d] and H_2O[c]) due to GG ionotropic sensitivity. Thus, like H^+, cations existing in the solutions in which hydrogels were soaked could interact with GG chains, promoting their aggregation and, therefore, lowering HGG medium uptake capacity (Coutinho et al., 2010; Moritaka et al., 1995).

3.4. Crosslinking density of the different HGGs

Besides, since crosslinking density (d_x) and average molecular weight between crosslinks (M_c) determine hydrogel swelling capacity and, therefore, hydrogel drug release patterns, d_x and M_c of the different HGGs were also determined based on the data obtained in the swelling tests once HGGs reach equilibrium in H_2O(d). The values calculated for these parameters, as well as for the different polymer volume fractions (V_r), are reported in Table S5.

As can be seen in the Supplementary Material, when greater concentrations of L-Cys were employed for HGG preparation, the average polymer volume fraction and molecular weight between crosslinkings diminished. By contrast and as expected, HGG crosslinking density increased. In this way, when greater amounts of crosslinker were

Table 1
HGG apparent porosity (%) and mean diameter (μm) ± SD of the macro- and micropores of the different hydrogel samples, once freeze-dried, determined *via* SEM image analysis.

Sample	Porosity (%)	Mean macropore size	Mean micropore size
HGG_{AB}[1.5LCys]	97.93 ± 1.4	553.1 ± 186.6 μm	325.9 ± 95.5 μm
HGG_{AB}[3LCys]	96.53 ± 2.1	550.3 ± 155.5 μm	215.7 ± 69.0 μm
HGG_{AB}[4.5LCys]	95.88 ± 1.7	561.0 ± 193.7 μm	225.6 ± 32.8 μm
HGG_{PBS}[1.5LCys]	93.01 ± 0.9	442.3 ± 95.9 μm	123.2 ± 48.4 μm
HGG_{PBS}[3LCys]	91.80 ± 1.6	354.3 ± 161.0 μm	123.0 ± 74.7 μm
HGG_{PBS}[4.5LCys]	90.50 ± 1.8	390.0 ± 91.9 μm	127.2 ± 48.0 μm

incorporated, the space for solvent accommodation between GG chains could be reduced, being this fact in agreement with the results previously obtained in the swelling tests.

3.5. Porosity of the different freeze-dried HGGs

Once the crosslinking degree of the different HGGs was analyzed, their apparent porosity was calculated and their morphology was studied by SEM. Fig. 3 shows the images obtained from all samples once freeze-dried and cross-sectioned, while Table 1 shows HGG mean apparent porosity and the average diameter of the hydrogel macro- and micropores, determined *via* image analysis.

As can be noticed in both, Fig. 3 and Table 1, the macro- and micropores of the HGG_{AB} samples were bigger than those of the HGG_{PBS} samples, which were less porous. In addition, as can be observed in the images, HGGs prepared in PBS had more micropores than those synthesized in AB, which again revealed their greater degree of crosslinking.

Likewise, regarding the diameter of the macro- and micropores of the HGGs prepared in AB with different concentrations of L-Cys, it should be noted that differences were not statistically significant in the case of macropores, but they were in the case of micropores, since those of the $HGGs_{AB}$[1.5LCys] were smaller than the micropores of the other hydrogels according to the *post hoc* analysis (Tukey test) that was later performed ($p < 0.05$). On the contrary, the differences in the size of the macropores of the $HGGs_{PBS}$ were more remarkable than those of the micropores. In this manner, the diameter of the micropores of all $HGGs_{PBS}$ was very similar, although as the concentration of L-Cys used in

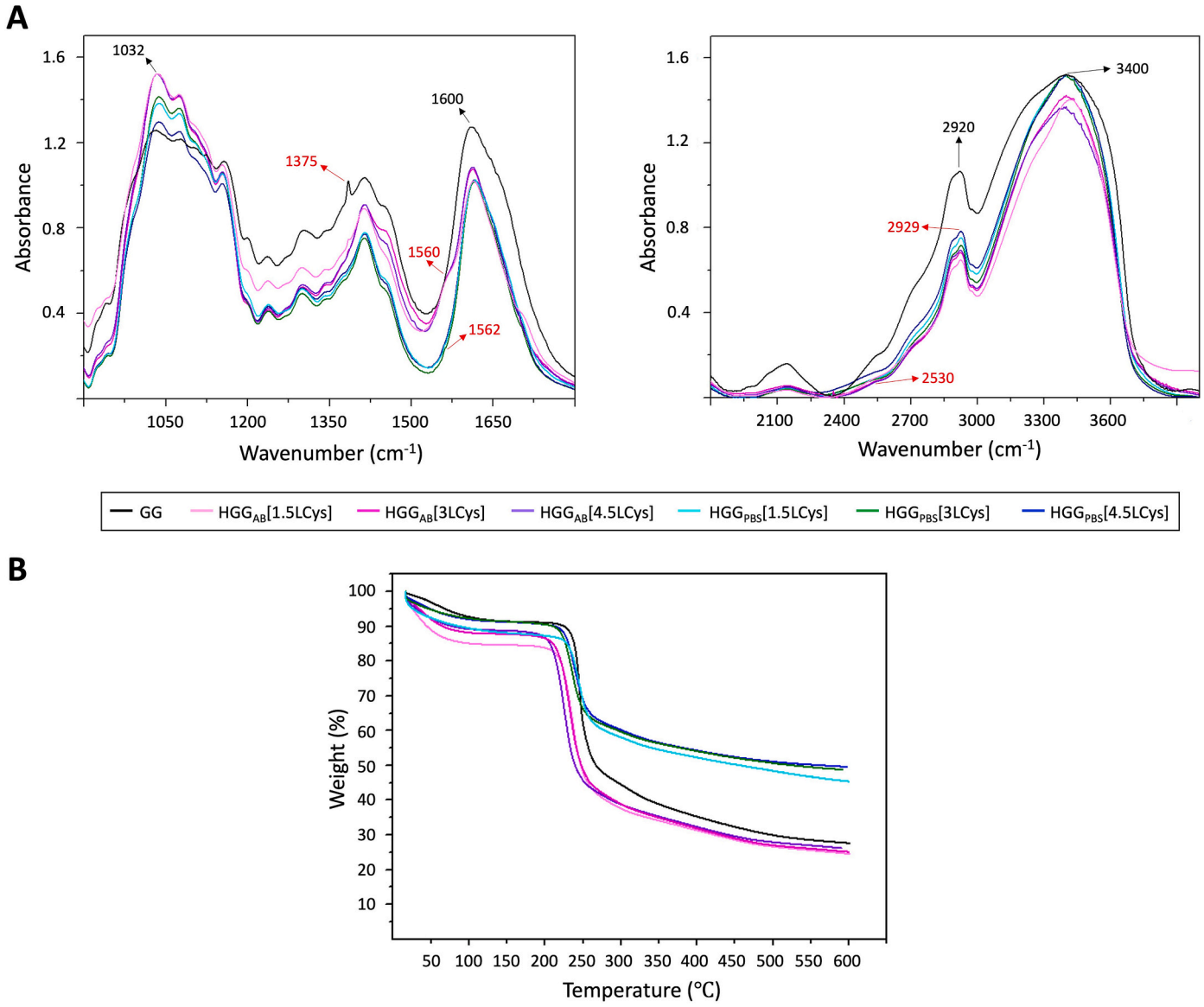

Fig. 4. (**A**) IR spectra of GG and the different HGGs in the 900–1800 cm^{-1} (left) and 1800–4000 cm^{-1} (right) ranges; (**B**) TG curves obtained for GG and the different HGGs.

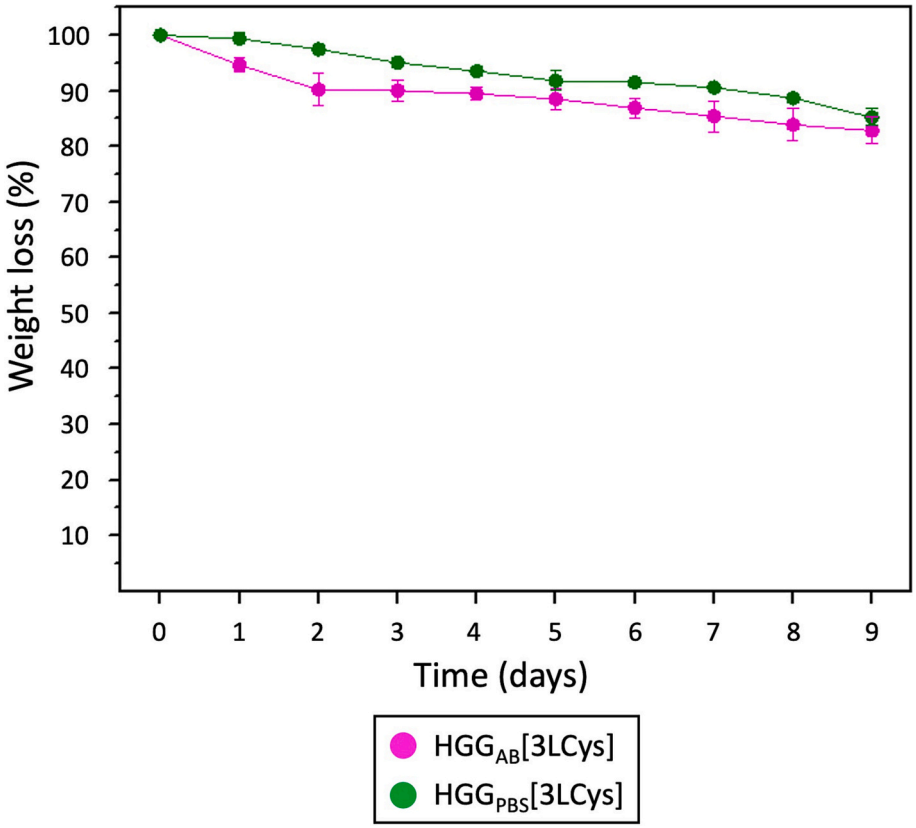

Fig. 5. Degradation rate of HGG$_{AB}$[3LCys] and HGG$_{PBS}$[3LCys] samples after incubation with lysozyme solutions (1 mg/ml) at 37 °C for 9 days.

hydrogel synthesis increased, they had greater number of micropores.

3.6. Chemical structure of the different HGGs

As can be seen in Fig. 4(A), all GG characteristics bands within the 900–4000 cm^{-1} range could be distinguished in the spectra of the different HGGs. In this manner, GG-specific peaks were observed at 1032 cm^{-1} (—C—O—C— stretching), 1600 cm^{-1} (C═O stretching vibrations), 2920 cm^{-1} (—CH stretching) and 3400 cm^{-1} (—OH stretching) in all samples (Lee et al., 2020). There were no significant differences between the spectra of the HGGs$_{AB}$ and those of the HGGs$_{PBS}$. Nevertheless, when comparing GG spectrum to the spectra of the hydrogels, some alterations (marked in red in Fig. 4[A]) could be appreciated, possibly indicative of HGG successfully crosslinking with L-Cys *via* EDC/NHS reaction. Herein, HGGs had a peak at 1560–1562 cm^{-1} that may correspond to the —CONH— amide bond formation between GG —COOH and L-Cys —NH groups, and which was not present in GG spectrum (Panczyszyn et al., 2021). The band at 1375 cm^{-1}, which could correspond to the C—H bending and which was marked in the GG spectrum (Criado et al., 2016), disappeared in the spectra of all HGGs. Finally, the characteristic peak of the -SH group was detected at 2530 cm^{-1}, and the peaks related to -CH$_2$ vibrations at 2920–2929 cm^{-1} were more pronounced for the HGGs in comparison with GG, which may confirm the thiolation of the hydrogels after L-Cys crosslinking (George et al., 2020; Xu et al., 2021).

3.7. Thermal stability of the different HGGs

A TGA of the six different types of HGGs prepared was performed to evaluate their thermal stability and mass loss and, thus, further corroborate their crosslinking degree, since differences in degradation temperatures can give some provision about polymer crosslinking. TG curves obtained for them can be seen in Fig. 4(B), along with the GG curve.

As can be noticed in Fig. 4(B), both GG and all HGGs showed a two-step thermogram, where the first stage of minor weight loss occurred in the 50–100 °C range. This weight loss was likely caused by the evaporation of the adsorbed buffer/H$_2$O in the samples. Thus, it may be directly related to HGG swelling capacity (Ding et al., 2021; Karthika & Vishalakshi, 2015) and, for this reason, it was greater for the HGG$_{AB}$ samples (11.1–14–4 %) than for the HGG$_{PBS}$ samples (8.5–11.0 %) and GG (8.6 %). Likewise, HGGs crosslinked with lower L-Cys concentrations lost greater weight than those prepared with higher concentrations of the crosslinker, fact that showed again that L-Cys concentration in samples had an inverse relationship with the swelling capacity of the hydrogels and, consequently, with their porosity.

On the other hand, the second stage of weight loss, which occurred in the 250–300 °C range, could account for GG degradation and the subsequent destruction of the whole hydrogel network structure (Ding et al., 2021; Karthika & Vishalakshi, 2015). At this stage, HGG$_{AB}$[1.5LCys], HGG$_{AB}$[3LCys] and HGG$_{AB}$[4.5LCys] samples lost about 50.6 %, 53 % and 53.7 % of weight, while HGG$_{PBS}$[1.5LCys], HGG$_{PBS}$[3LCys] and HGG$_{PBS}$[4.5LCys] samples lost about 30.8 %, 32.4 % and 33.3 % of weight, respectively. Thereby, the overall trend showed that the greater the degree of HGG crosslinking, the smaller their rate of weight loss and the better their thermal stability.

3.8. Compression modulus of HGGs[3LCys]

The swelling and deswelling capacity of the hydrogels, which is determined by their crosslinking degree, governs drug release. In this way, greater crosslinking degrees reduce hydrogel pore size and deswelling capacity and decrease the overall diffusion of the drugs through the polymer networks (Khan & Ranjha, 2014; Sivakumaran et al., 2013). Therefore, based on the results obtained up to this point, it was considered that using HGGs[1.5LCys] could lead to a quick burst release

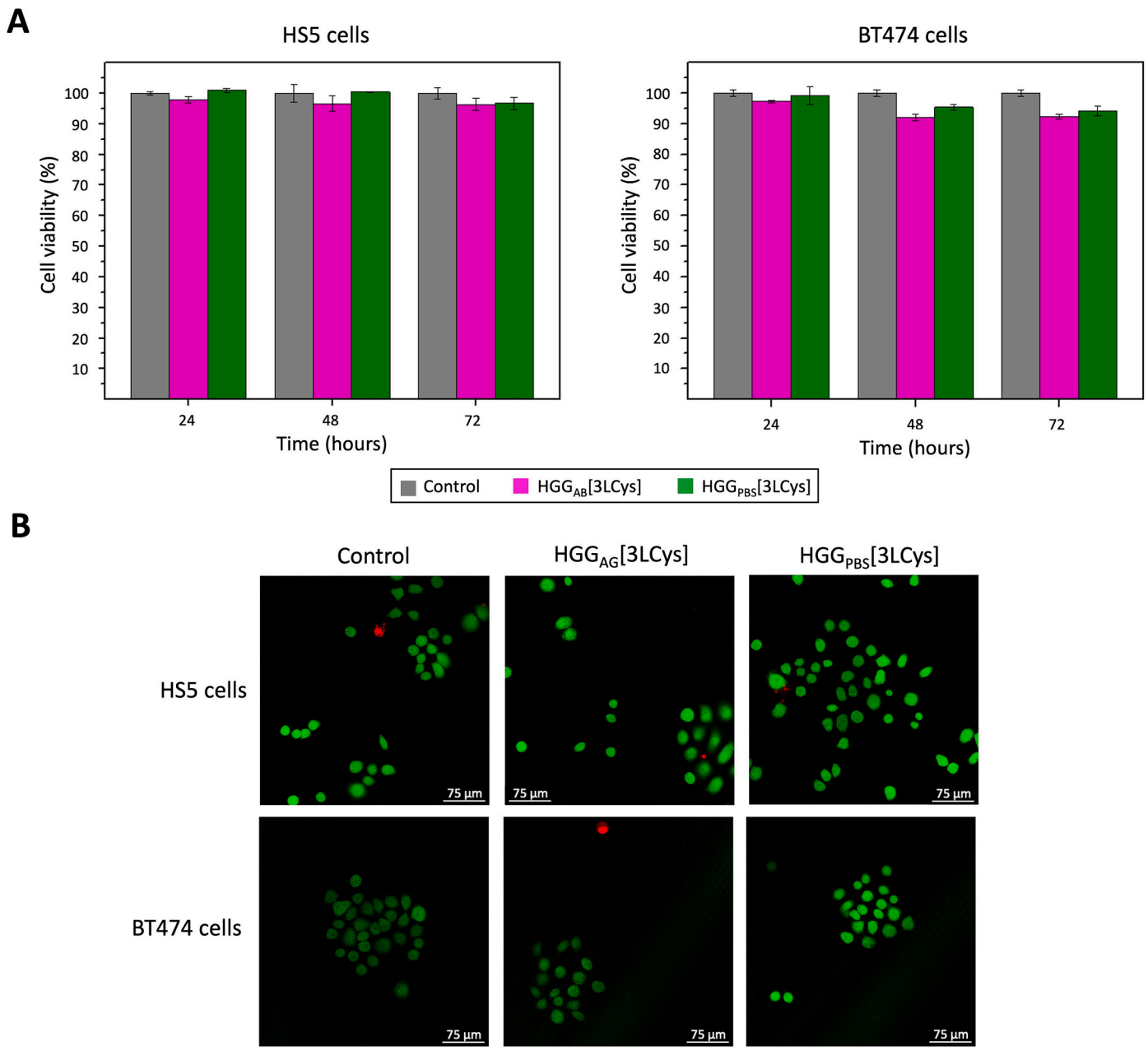

Fig. 6. (**A**) Results of the MTT assays performed with HS5 and BT474 cells to assess HGG biocompatibility. Cells were exposed to both HGGs$_{AB}$[3LCys] and HGGs$_{PBS}$[3LCys] (23.1 % [*v*/v]), and their relative viability was compared with that of an untreated control. The results shown are the average viability values ± SD of three independent samples; (**B**) CLSM images of HS5 and BT474 cells 24 h after exposure to HGGs[3LCys] (23.1 % [v/v]). Cell survival and death were assessed by using calcein AM (green) and propidium iodide (red).

of PTX due to their larger pore size (Sivakumaran et al., 2013), while PTX release from HGGs[4.5LCys] may be too slow because of their elevated number of micropores. Herein, those HGGs crosslinked with 3 mg/ml L-Cys were regarded to be the most suitable hydrogels to achieve proper, local PTX release, and they were chosen to perform subsequent assays.

Therein, mechanical properties of the HGGs[3LCys] were analyzed using static compression measurements. The average Young's modulus of both HGGs$_{AB}$[3LCys] and HGGs$_{PBS}$[3LCys] was found to be 86.5 ± 12.9 KPa and 95.9 ± 7.8 KPa, respectively. Despite being close values ($p > 0.05$), slightly increased mechanical strength in HGGs$_{PBS}$ was expected because of their higher degree of crosslinking. In any case, the compression elastic moduli of both hydrogels were in the range of the modulus compression elasticity of most biological tissues that are soft viscoelastic materials (0.1–100 KPa) (Shpaisman et al., 2012), so they could meet the requirements to potentially be applied *in vivo* in the future.

3.9. Enzymatic degradation rate of HGGs[3LCys]

Before proceeding to load HGGs[3LCys] with the PTX:βCD complexes, their biosuitability was first analyzed using enzymatic degradation assays. The results obtained when investigating the degradation behavior of the HGGs$_{AB}$[3LCys] and the HGGs$_{PBS}$[3LCys] after incubation with lysozyme solutions can be seen in Fig. 5.

As can be observed in Fig. 5, the weight of both hydrogel types decreased gradually with incubation time increasing, which proved their biodegradability. Nonetheless, compared to HGGs$_{PBS}$[3LCys],

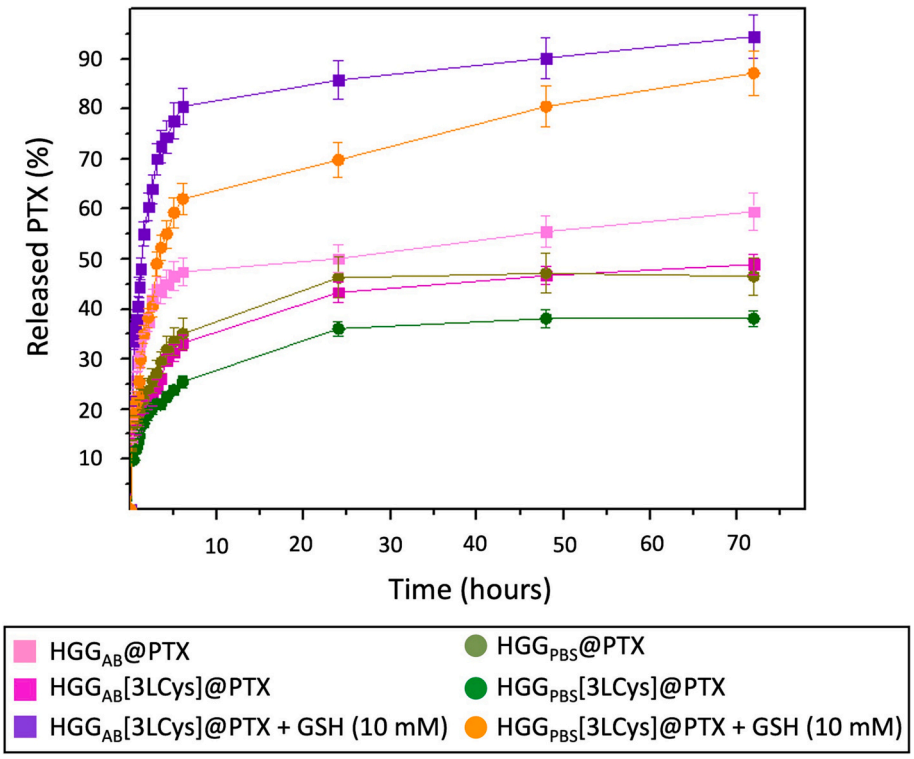

Fig. 7. *In vitro* drug delivery profile of HGG@PTX and HGG[3LCys]@PTX samples at 37 °C and pH 6.8, under conditions of high GSH concentrations or not.

HGG_{AB}[3LCys] samples showed a slightly higher degradation rate. Thus, hydrogels prepared in AB were able to uptake a greater volume of lysozyme solution than those synthesized in PBS, and this revealed again that they had a lower degree of crosslinking and greater porosity (Huang et al., 2020). Herein, this fact also agreed with the results obtained in previous experiments.

3.10. HGG[3LCys] cytocompatibility in vitro

To continue verifying HGGs[3LCys] biosuitability, their cytocompatibility was also studied, since it is crucial for their potential clinical application as therapeutics. For this purpose, both colorimetric assays and live/dead staining were performed with stromal (HS5) and HER2+ breast carcinoma cells (BT474).

The results obtained in the MTT assays are depicted in Fig. 6(A). As can be noticed, neither exposure to $HGGs_{AB}$[3LCys] nor exposure to $HGGs_{PBS}$[3LCys] significantly reduced the relative viability of HS5 or BT474 cells as compared to the control ($p > 0.05$). Consequently, regardless of having been prepared in AB or PBS, HGGs[3LCys] seemed to have adequate cytocompatibility, since stromal and breast cancer cell viabilities were superior to 90 % throughout the studied time (72 h).

The live/dead CLSM assays carried out also showed the absence of cytotoxicity of both HGGs[3LCys] for 24 h (Fig. 6[B]), since exposure to them did not cause the viability of neither BT474 nor HS5 cells to decrease as compared to the untreated control.

3.11. PTX release from HGGs[3LCys]

The combination of the unique characteristics of hydrogels makes them very useful in drug delivery applications. These 3D networks can imbibe large volumes of aqueous solutions due to their hydrophobicity and porous structure. For this reason, some drug release mechanisms can occur simultaneously, such as diffusion because of the penetration of water molecules inside the matrix, swelling of the matrix and/or dissolution or erosion of the matrix (Lin & Metters, 2006; Permanadewi et al., 2019).

Fig. 7 shows the cumulative release profile at the tumor extracellular pH (pH 6.8) of both $HGGs_{AB}$[3LCys] and $HGGs_{AB}$[3LCys] once loaded with the PTX:βCD complexes. This profile was compared to that of non-crosslinked $HGGs_{AB}$ and $HGGs_{PBS}$ loaded with the same concentrations of the taxane inclusion complexes and to the release prolife of HGG[3LCys]@PTX samples that were kept under conditions of high GSH concentrations (10 mM).

As can be noticed, there was a slight burst release, which is commonly observed for biodegradable polymeric systems (Albisa et al., 2017), from all hydrogel samples up to 6 h. After this time, PTX release ratio of $HGGs_{AB}$[3LCys]@PTX and $HGGs_{PBS}$[3LCys]@PTX was close to 33 % and 25.5 %, respectively, while PTX release ratio of $HGGs_{AB}$@PTX and $HGGs_{PBS}$@PTX was close to 47.5 % and 35 %. Later, successive sustained release patterns occurred and, over 72 h, about 49 % of the taxane was release from the crosslinked hydrogels synthesized in AB, while about 38 % was released from the crosslinked hydrogels prepared in PBS. Thereby, PTX release rate of the $HGGs_{AB}$[3LCys]@PTX was a little faster than that of the $HGGs_{PBS}$[3LCys]@PTX in acidic PBS (pH 6.8), possibly because the $HGGs_{PBS}$ had greater crosslinking density and, hence, more limited swelling capacity (Saidi et al., 2020). Likewise, it was shown that PTX release rate of the crosslinked hydrogels was more controlled than that of the non-crosslinked samples (which released 59.5–47 % PTX after 72 h) but, in both cases, PTX release was incomplete. In contrast, when $HGGs_{AB}$[3LCys]@PTX and $HGGs_{PBS}$[3LCys]@PTX were immersed in release medium containing high concentrations of GSH, practically all (87–95 %) the taxane contained in the samples was released over 72 h, which proved that L-Cys-based crosslinking conferred redox-responsive properties to the HGGs.

To investigate the mechanism that was responsible for PTX release from the HGGs@PTX and HGGs[3LCys]@PTX in the presence and absence of high GSH concentrations or not, the experimental data obtained were fitted through several typical mathematical models. The release constants (K), coefficients of correlation (R) and diffusion exponents (n) obtained can be found in the Supplementary Material (Table S6). According to the R^2 values achieved, among all the studied models, the Korsmeyer-Peppas model was the best fit ($R^2 > 95$ %) for

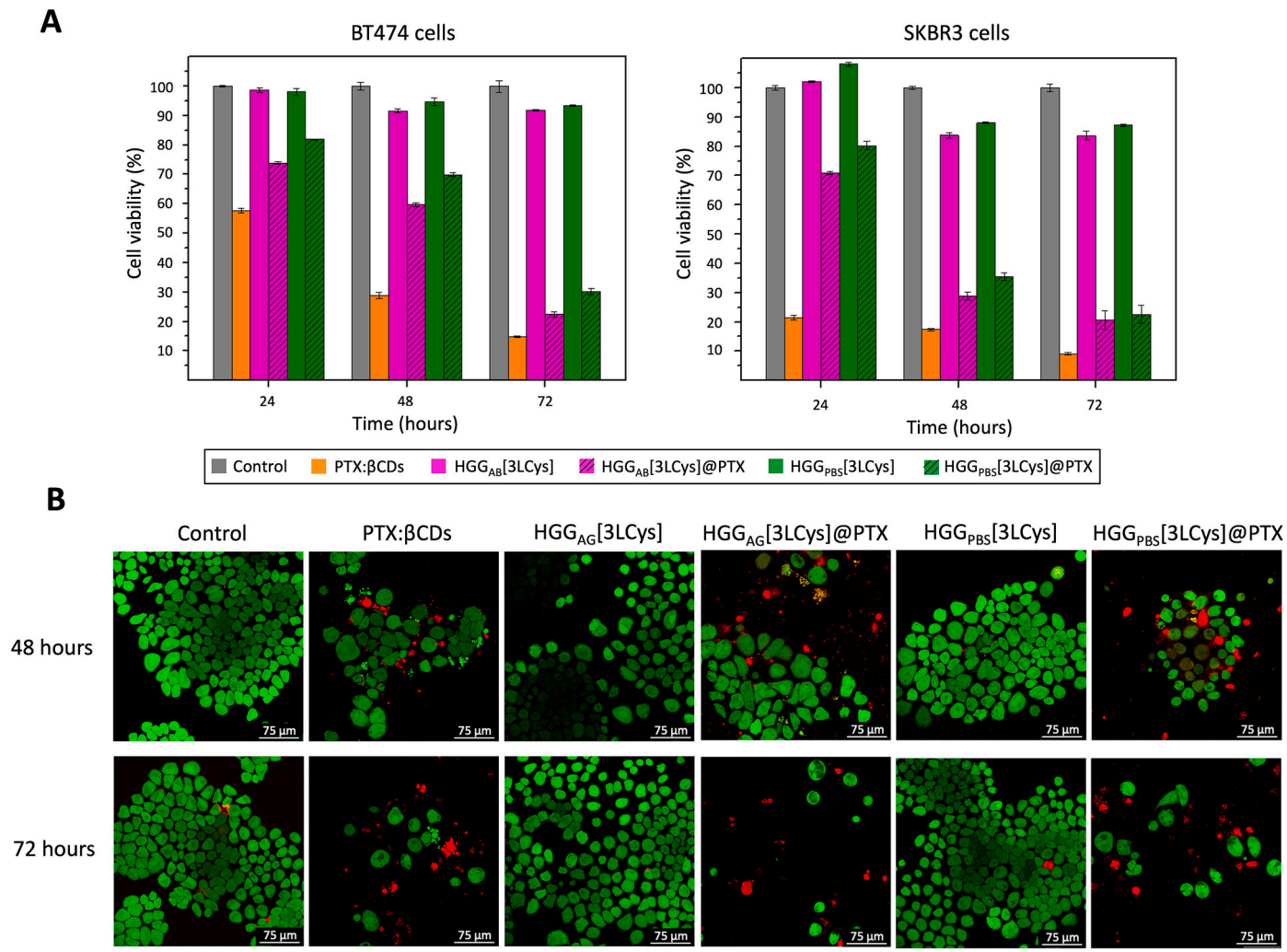

Fig. 8. (**A**) Results of the MTT assays performed with BT474 and SKBR3 cells to assess the antiproliferative activity of the HGGs[3LCys]@PTX. Tumor cells were exposed to the two types of HGGs[LCys] and HGGs[3LCys]@PTX (23.1 % [*v*/v]) prepared and to PTX:βCDs in the same concentration as that loaded (30.8 μM) in the HGGs. Again, the results shown are the average viability values ± SD of three independent samples; (**B**) CLSM images of BT474 cells 48 and 72 h after exposure to the same concentrations of HGGs[3LCys], HGGs[LCys]@PTX, and PTX:βCDs as in the MTT assays. Cell survival and death were again assessed by using calcein AM (green) and propidium iodide (red), respectively.

PTX release from the HGGs. According to this model, since diffusion exponent values were similar for both types of non-crosslinked and crosslinked HGG and inferior to 0.45 (0.2478 and 0.2568), PTX was presumably released from all the samples by quasi-Fickian diffusion (Vigata et al., 2020).

3.12. Antitumor activity of HGGs[3LCys]@PTX

The antiproliferative activity of HGG$_{AB}$[3LCys]@PTX and HGG$_{PBS}$[3LCys]@PTX samples was assessed *in vitro*. Both MTT assays and live/dead staining were performed on this occasion, too, but two HER2-overexpressing breast carcinoma cell lines were employed: BT474 and SKBR3 (Nieto et al., 2019). In addition, LDH detection assays were carried out to analyze the membrane integrity of both types of breast cancer cells after HGG[3LCys]@PTX treatment, since LDH is a cytosolic enzyme released when cellular membrane is damaged (Madani et al., 2020). The results obtained can be found in Figs. 8 and S2.

Regarding the results obtained in the MTT assays (Fig. 8[A]), it was noticed that the viability rate of both types of breast cancer cells was reduced gradually over time when treated with the HGGs[3LCys]@PTX. In this way, the BT474 viability rate decreased to 22 % after treatment with the HGGs$_{AB}$[3LCys]@PTX for 72 h, and to 28 % when cells were exposed to the HGGs$_{PBS}$[3LCys]@PTX. Meanwhile, the SKBR3 viability rate decreased to 19 % and 21 % 72 h after treatment with the HGGs$_{AB}$[3LCys]@PTX and HGGs$_{PBS}$[3LCys]@PTX, respectively. After the same time, PTX:βCD treatment achieved to decrease the viability rate of BT474 and SKBR3 cells to 14 % and 9 %, respectively. Thus, the reduction of breast cancer cell viability caused by the PTX-loaded HGGs was not as high as in the case of the treatment with the taxane complexes ($p < 0.05$), but GG patches turned out to be also highly effective and, in fact, helped to achieve more controlled PTX release in cancer cell cytoplasm, where GSH concentrations are several times higher than in normal cells (Kumar et al., 2015). Besides, results agreed with those obtained when analyzing PTX release kinetics *in vitro*, since treatment with the loaded HGGs$_{AB}$, which showed lower crosslinking degree and faster PTX release, managed to reduce breast cancer cell viability slightly more noticeably (3–10 % more) than the HGGs$_{PBS}$[3LCys]@PTX.

The live/dead staining assays corroborated the results obtained with the MTT assays. As can be seen in Fig. 8(B), similar to the PTX:βCDs administered, both types of PTX-loaded hydrogels significantly reduced the number of viable HER2+ tumor cells compared to the untreated control after 48 and 72 h of exposure.

At last, LDH colorimetric assays showed that when BT474 and SKBR3

cells were exposed to $HGGs_{AB}$[3LCys]@PTX and $HGGs_{PBS}$[3LCys]@PTX for 48 h (Fig. S2), the amount of the LDH released was significantly greater (almost double) than that released by the controls ($p < 0.05$) (Fig. S2) and, therefore, that breast cancer cell membrane integrity was affected by HGG[3LCys]@PTX treatment.

Thereby, all these results highlighted the potential of the PTX-loaded HGGs for local implantation *in vivo* after tumor resection, with the possibility of adjusting the taxane release rate as necessary, simply by modifying HGG crosslinking densities.

4. Conclusions

In summary, GG-based implantable hydrogels with different degrees of chemical crosslinking were successfully prepared in two different buffers for local, redox-responsive PTX release using an approach that has not been previously described: post-surgery treatment of HER2+ breast tumors. Hydrogel dynamic modulus, equilibrium swelling rate, pore characteristics and thermal stability could be adjusted by synthesizing them in AB or PBS and by modifying the concentration of L-Cys used for their crosslinking. Those hydrogels with a medium degree of crosslinking, which were considered more appropriate for drug release applications, were selected to carry out *in vitro* assays. They proved to have adequate mechanical properties for potential tissue support. In addition, these hydrogels showed appropriate biodegradability and good cell tolerance and, when loaded with PTX:βCD complexes, were able to achieve a GSH-controlled release of the taxane. Likewise, PTX-loaded HGGs proved to have promising antiproliferative activity *in vitro* when validated with HER2+ breast carcinoma cell lines. Thus, PTX-loaded HGGs could be considered for future *in vivo* and pre-clinical studies to accomplish local PTX accumulation in breast tumor tissues, avoiding systemic effects while reducing the incidence of tumor relapse.

Abbreviations

AB	Acetate buffer
βCD	β-cyclodextrin
DDS	Drug delivery system
GG	Gellan gum
GSH	Glutathione
HGG	Gellan gum hydrogel
HGG_{AB}	Gellan gum hydrogel prepared in acetate buffer
HGG_{PBS}	Gellan gum hydrogel prepared in PBS
HGG[1.5LCys]	Gellan gum hydrogel crosslinked with 1.5 mg/ml L-cysteine
HGG[3LCys]	Gellan gum hydrogel crosslinked with 3 mg/ml L-cysteine
HGG[4.5LCys]	Gellan gum hydrogel crosslinked with 4.5 mg/ml L-cysteine
HGG_{AB}[3LCys]@PTX	Gellan gum hydrogel prepared in acetate buffer, crosslinked with 3 mg/ml L-cysteine and loaded with paclitaxel:β-cyclodextrin inclusion complexes
HGG_{PBS}[3LCys]@PTX	Gellan gum hydrogel prepared in PBS, crosslinked with 3 mg/ml L-cysteine and loaded with paclitaxel:β-cyclodextrin inclusion complexes
L-Cys	L-cysteine
LDH	Lactate dehydrogenase
PTX	Paclitaxel
PTX:βCDs	Paclitaxel:β-cyclodextrin inclusion complexes

CRediT authorship contribution statement

Celia Nieto: Conceptualization, Methodology, Investigation, Validation, Supervision, Writing – original draft, Writing – review & editing. **Milena A. Vega:** Conceptualization, Investigation, Software, Supervision, Writing – review & editing. **Víctor Rodríguez:** Investigation. **Patricia Pérez Esteban:** Resources, Supervision, Writing – review & editing. **Eva M. Martín del Valle:** Writing – review & editing, Supervision, Project administration, Funding acquisition.

Declaration of competing interest

The authors declare no competing financial interest.

Acknowledgements

This work was financially supported by Spanish Ministry of Sciences, Innovation and Universities (PID2019-108994RB-I00). In addition, the authors thank the Microscopy Unit of the University of Valladolid for the SEM images, and the Thermal Analysis Laboratory of the Complutense University for the TGA.

Appendix A. Supplementary data

Supplementary data to this article can be found online at https://doi.org/10.1016/j.carbpol.2022.119732.

References

Abasalizadeh, F., Moghaddam, S. V., Alizadeh, E., Akbari, E., Kaskani, E., Fazljou, S. M. B., Tortabi, M., & Akborzadeh, A. (2020). Alginate-based hydrogels as drug delivery vehicles in cancer treatment and their application in wound dressing and 3D bioprinting. *Journal of Biological Engineering, 14*, 8.

Afinjuomo, F., Barclay, T. G., Song, Y., Parikh, A., Petrovsky, N., & Garg, S. (2019). Synthesis and characterization of a novel inulin hydrogel crosslinked with pyromellitic dianhydride. *Reactive and Functional Polymers, 134*, 104–111.

Albisa, A., Piacentini, E., Sebastian, V., Arruebo, M., Santamaria, J., & Giorno, L. (2017). Preparation of drug-loaded PLGA-PEG nanoparticles by membrane-assisted nanoprecipitation. *Pharmaceutical Research, 34*, 1296–1308.

Alcaro, S., Ventura, C. A., Paolino, D., Battaglia, D., Ortuso, F., Cattel, L., Puglisi, G., & Fresta, M. (2002). Preparation, characterization, molecular modeling and in vitro activity of paclitaxel-cyclodextrin complexes. *Bioorganic & Medicinal Chemistry Letters, 12*, 1637–1641.

Askari, E., Seyfoori, A., Amereh, M., Gharaie, S. S., Ghazali, H. S., Ghazali, Z. S., Khunjush, B., & Akbari, M. (2020). Stimuli-responsive hydrogels for local post-surgical drug delivery. *Gels, 6*, 14.

Bacelar, A. H., Silva-Correia, J., Oliveira, J. M., & Reis, R. L. (2016). Recent progress in gellan gum hydrogels provided by functionalization strategies. *Journal of Material Chemistry B, 4*, 6164.

Bastiancich, C., Bianco, J., Vanvarenberg, K., Ocakar, B., Joudiou, N., Galliz, B., Bastiat, G., Lagarce, F., Préat, V., & Danhier, F. (2017). Injectable nanomedicine hydrogel for local chemotherapy of glioblastoma after surgical resection. *Journal of Controlled Release, 264*, 45–54.

Bu, L.-L., Yan, J., Wang, Z., Ruan, H., Chen, Q., Gunadhi, V., Bell, R. B., & Gu, Z. (2019). Advances in drug delivery for post-surgical cancer treatment. *Biomaterials, 219*, Article 119182.

Cassanelli, M., Prosapio, V., Norton, I., & Mills, T. (2018). Acidified/basified gellan gum gels: The role of the structure in drying/rehydratation mechanisms. *Food Hydrocolloids, 82*, 346–354.

Coutinho, D. F., Sant, S. V., Shin, H., Oliveira, J. T., Gomes, M. E., Neves, N. M., Khademhosseini, A., & Reis, R. L. (2010). Modified gellan gum hydrogels with tunable physical and mechanical properties. *Biomaterials, 31*, 7494–7502.

Criado, P., Fraschini, C., Salmieri, S., Becher, D., Safrany, A., & Lacroix, M. (2016). Free radical grafting of gallic acid (GA) on cellulose nanocrystals (CNCS) and evaluation of antioxidant reinforce gellan gum films. *Radiation Physics and Chemistry, 118*, 61–69.

D'Arrigo, G., Navarro, G., Di Meo, C., Matricardi, P., & Torchilin, V. (2014). Gellan gym nanohydrogels containing anti-inflammatory and anti-cancer drugs: A multi-drug delivery system for a combination therapy in cancer treatment. *European Journal of Pharmaceutics and Biopharmaceutics, 87*(1), 208–216.

Darge, H. F., Andrgie, A. T., Tsai, H.-C., & Lai, J.-Y. (2019). Polysaccharide and polypeptide based injectable thermosensitive hydrogels for local biomedical applications. *International Journal of Biological Macromolecules, 133*, 545–563.

Das, M., & Giri, T. K. (2020). Hydrogels based on gellan gum in cell delivery and drug delivery. *Journal of Drug Delivery Science and Technology, 56*, Article 101586.

De Souza, F. S., de Mello Ferreira, I. L., da Silva Costa, M. A., Ferreira de Lima, A. L., Melo da Costa, M. P., & Monteiro da Silva, G. (2016). Evaluation of different methods to prepare superadsorbent hydrogels base don deactylated gellan. *Carbohydrate Polymers, 148*, 309–317.

Ding, L., Song, S., Chen, L., Shi, J., Zhao, B., Teng, G., & Zhang, J. (2021). A freeze-thawing method applied to the fabrication of 3-d curdlan/polyvinyl alcohol hydrogels as scaffolds for cell culture. *International Journal of Biological Macromolecules, 174*, 101–109.

Du, H., Halmiton, P., Reilly, M., & Ravi, N. (2012). Injectable in situ physically and chemically crosslinkable gellan hydrogel. *Macromolecular Bioscience, 12*(7), 952–961.

Fang, Y., Wang, K., Li, Q., & Huang, C. (2021). pH responsive release of paclitaxel by self-assembling chitosan-ethyl vanillin@GNRs nanocomposites. *International Journal of Pharmaceutics, 607*, Article 121047.
Ganji, F., Vasheghani, F., & Vasheghani, F. (2010). Theoretical description of hydrogel swelling: A review. *Iranian Polymer Journal, 19*(5), 375–398.
George, D., Maheswari, U., & Sheriffa Begum, K. M. M. (2020). Cysteine conjugated based green nanohybrid hydrogel embedded with zinc oxide nanoparticles towards enhanced therapeutic potential of naringenin. *Reactive and Functional Polymers, 148*, Article 104480.
Goodarzi, H., Jadidi, K., Pourmotabed, S., Sharifi, E., & Aghamollaei, H. (2019). Preparation and in vitro characterization of cross-linked collagen-gelatin hydrogel using EDC/NHS for corneal tissue engineering applications. *International Journal of Biological Macromolecules, 126*, 620–632.
GuhaSarkar, S., More, P., & Banerjee, R. (2017). Urothelium-adherent ion-triggered liposome-in-gel system as a platform for intravesical drug delivery. *Journal of Controlled Release, 245*, 147–156.
Hua, J., Li, Z., Xia, W., Yang, N., Gong, J., Zhang, J., & Qiao, C. (2016). Preparation and properties of EDC/NHS mediated crosslinking poly(gamma-polylysine) hydrogel. *Material Science Engineering C, 61*, 879–892.
Huan, Y., Kong, Q., Tang, Q., Wang, Y., Mou, H., Ying, R., & Li, C. (2022). Antimicrobial peptides/ciprofloxacin-loaded O-carboxymethyl chitosan/self-assembling peptides hydrogel dressing with sustained-release effect for enhanced anti-bacterial infection and wound healing. *Carbohydrate Polymers, 280*, Article 119033.
Huang, S., Chen, H.-J., Deng, Y.-P., You, X.-H., Fang, Q.-H., & Lin, M. (2020). Preparation of noble stable microbicidal hydrogel films as potential wound dressing. *Polymer Degradation and Stability, 181*, Article 109349.
Kang, M. S., Kong, T. W. S., Khoo, J. Y. X., & Loh, T.-P. (2021). Recent developments in chemical conjugation strategies targeting native amino acids in proteins and their applications in antibody drug conjugates. *Chemical Science Journal, 12*, 13613.
Karthika, J. S., & Vishalakshi, B. (2015). Novel stimuli responsive gellan gum-graft-poly (DMAEMA) hydrogel as adsorbent for anionic dye. *International Journal of Biological Macromolecules, 81*, 648–655.
Khan, S., & Ranjha, N. M. (2014). Effect of degree of cross-linking on swelling and on drug release of low viscous chitosan/poly (vinyl alcohol) hydrogels. *Polymer Bulletin, 71*, 2133–2158.
Kibria, G., & Hatakeyama, H. (2014). Cancer multidrug resistance: Mechanisms involved and strategies for circumvention using a drug delivery system. *Archives of Pharmacal Research, 37*, 4–15.
Kumar, A., Lale, S. V., Mahajan, S., Choudhary, V., & Koul, V. (2015). ROP and ATPR fabricated dual targeted redox sensitive polymerosomes based on pPEGMA-PCL-ss-PCL-pPEGMA triblock copolymers for breast cancer therapeutics. *ACS Applied Materials & Interfaces, 7*, 9211–9227.
Lee, S., Hee Choi, J., Park, A., Rim, M., Youn, J., Lee, W., Song, J. E., & Khang, G. (2020). Advanced gellan gum-based glycol chitosan hydrogel for cartilage tissue engineering biomaterial. *International Journal of Biological Macromolecules, 158*, 452–460.
Li, Y., Hou, X., Pan, Y., Wang, L., & Xiao, H. (2020). Redox-responsive carboxymethyl cellulose hydrogel for adsorption and controlled release of a dye. *European Polymer Journal, 123*, Article 109447.
Li, L., Guo, J., & Xiong, R. (2021). Synthesis and swelling behaviour of a fully degradable physical cross-linked high strength hydrogel. *Polymer Testing, 94*, Article 106982.
Lin, C.-C., & Metters, A. T. (2006). Hydrogels in controlled release formulations: Network design and mathematical modeling. *Advanced Drug Delivery Reviews, 58*, 1379–1408.
Lu, S., Kong, S., Wang, Y., Hu, Z., Zhang, L., & Liao, M. (2022). Gastric acid-response chitosan/alginate/tilapia collagen peptide composite hydrogel: Protection effects on alcohol-induced gastric mucosal injury. *Carbohydrate Polymers, 277*, Article 118816.
Madani, F., Esnaashari, S. S., Bergonzi, M. C., Webster, T. J., Younesm, H. M., Khosravani, M., & Adabi, M. (2020). Paclitaxel/methotrexate co-loaded PLGA nanoparticles in glioblastoma treatment: Formulation development and in vitro antitumor activity evaluation. *Life Sciences, 256*, Article 117943.
Matricardi, P., Cencetti, C., Ria, R., Alhaique, F., & Coviello, T. (2009). Preparation and characterization of novel gellan gum hydrogels suitable for modified drug release. *Molecules, 14*, 3376–3391.
Misra, R., & Acharya, S. (2021). Smart nanotheranostic hydrogels for on-demand cancer management. *Drug Discovery Today, 26*(2), 344–359.
Morello, G., Quarta, A., Gaballo, A., Moroni, L., Gigli, G., Polini, A., & Gervaso, F. (2021). A thermo-sensitive chitosan/pectin hidrogel for long-term tumor spheroid culture. *Carbohydrate Polymers, 274*, Article 118633.
Moritaka, H., Nishinari, K., Taki, M., & Fukuba, H. (1995). Effects of pH, potassium chloride, and sodium chloride on the thermal and rheological properties of gellan gum hydrogels. *Journal of Agricultural and Food Chemistry, 43*, 1685–1689.
Nieto, C., Centa, A., Rodríguez-Rodríguez, J. A., Pandiella, A., & Martín del Valle, E. M. (2019). Paclitaxel-trastuzumab mixed nanovehicle to target HER2-overexpressing tumors. *Nanomaterials, 9*(7), 948.
Ning, L., You, C., Zhang, Y., Li, X., & Wang, F. (2020). Synthesis and biological evaluation of surface-modified nanocellulose hydrogel loaded with paclitaxel. *Life Sciences, 241*, Article 117137.
Oliveira, M. B., Custódio, C. A., Gasperini, L., Reis, R. L., & Mano, J. F. (2016). Autonomous osteogenic differentiation of hASCs encapsulated in methacrylated gellan-gum hydrogels. *Acta Biomaterialia, 41*, 119–132.
Pacelli, S., Basu, S., Berkland, C., Wang, J., & Paul, A. (2018). Design of a cytocompatible hydrogel coating to modulate properties of ceramic-based scaffolds for bone repair. *Cellular and Molecular Bioengineering, 11*(3), 211–217.
Palumbo, F. S., Federico, S., Pitarresi, G., Fiorica, C., & Giammona, G. (2020). Gellan gum-based delivery systems of therapeutic agents and cells. *Carbohydrate Polymers, 229*, Article 115430.
Panczyszyn, E., Jasko, M., Milek, O., Niedziela, M., Mecik-Kronenberg, T., Hoang-Bujnowicz, A., Zieba, M., Adamus, G., Kowalczuk, M., & Osyczka, A. M. (2021). Gellan gum hydrogels cross-linked with carbodiimide stimulates vacuolation of human tooth-derived stems cells in vitro. *Toxicology in Vitro, 73*, Article 105111.
Panpinit, S., Pongsomboon, S.-A., Keawin, T., & Saengsuwan, S. (2020). Development of multicomponent interpenetrating polymer network (IPN) hydrogel films based on 2-hydroxyethyl methacrylate (HEMA), acrylamide (AM), polyvinyl alcohol (PVA) and chitosan (CS) with enhanced mechanical strengths, water swelling and antibacterial properties. *Reactive and Functional Polymers, 156*, Article 104739.
Pelegri-O'Day, E. M., Lin, E.-W., & Maynard, H. D. (2014). Therapeutic protein-polymer conjugates: Advancing beyond PEGylation. *Journal of the American Chemical Society, 136*, 14323–14332.
Pérez, E., Fernández, A., Olmo, R., Teijón, J. M., & Blanco, M. D. (2014). pH and gluthation-responsive hydrogel for localized delivery of paclitaxel. *Colloids and Surfaces B: Biointerfaces, 116*, 247–256.
Permanadewi, I., Kumoro, A. C., Wardhani, D. H., & Aryanti, N. (2019). Modelling of controlled drug release in gastrointestinal tract simulation. *Journal of Physics: Conference Series, 1295*, Article 012063.
Prajapati, V. D., Jani, G. K., Zala, B. S., & Khutliwala, T. A. (2013). An insight into the emerging exopolysaccharide gellan gum as a novel polymer. *Carbohydrate Polymers, 93*, 670–678.
Qu, Y., Chu, B. Y., Peng, J. R., Liao, J. F., Qi, T. T., Shi, K., Zhang, X. N., Wei, Y. Q., & Qian, Z. Y. (2015). A biodegradable thermo-responsive hybrid hydrogel: Therapeutic applications in preventing the post-operative recurrence of breast cancer. *NPG Asia Materials, 7*, Article e207.
Rahnama, H., Khorasani, S. N., Aminoroaya, A., Molavian, M. R., Allafchian, A., & Khalili, S. (2021). Facile preparation of chitosan-dopamine-inulin aldehyde hydrogel for drug delivery application. *International Journal of Biological Macromolecules, 185*, 716–724.
Rezk, A. I., Obiweluozor, F. O., Choukrani, G., Park, C. H., & Kim, C. S. (2019). Drug release and kinetic models for anticancer drug (BTZ) from a pH-responsive alginate polydopamine hydrogel: Towards cancer chemotherapy. *International Journal of Biological Macromolecules, 14*, 388–400.
Richa, & Choudhury, A. R. (2019). Synthesis and rheological characterization of a novel thermostable quick setting composite hydrogel of gellan and pullulan. *International Journal of Biological Macromolecules, 125*, 979–988.
Robby, A. I., Lee, G., Lee, K. D., Jang, Y. C., & Park, S. Y. (2021). GSH-responsive self-healable conductive hydrogel of highly selective strain-pressure sensor for cancer cell detection. *NanoToday, 39*, Article 101178.
Roberts, M. C., Hanson, M. C., Massey, A. P., Karren, E. A., & Kiser, P. F. (2007). Dynamically restructuring hydrogel networks formed with reversible covalent crosslinks. *Advanced Materials, 19*, 2503–2507.
Sabadini, R. C., Silva, M. M., Pawlicka, A., & Kanicki, J. (2018). Gellan gum-O, O'-bis (2-aminopropyl)-polyethylene glycol hydrogel for controller fertilizer release. *Journal of Applied Polymer Science, 135*, 45636.
Safronov, A. P., Adamova, L. V., & Kurlyandskaya, G. V. (2019). Flory-huggings parameters of guar gum, xantham gum, agarose, and gellan gum in aqueous solutions. *Polymer Science, 61*(1), 29–38.
Saidi, M., Dabbaghi, A., & Rahmani, S. (2020). Swelling and drug delivery kinetics of click-synthesized hydrogels based on various combinations of PEG and star-shaped PCL: Influence of network parameters on swelling and release behaviour. *Polymer Bulletin, 77*, 3989–4010.
Schott, H. (1992). Kinetics of swelling of polymers and their gels. *Journal of Pharmaceutical Sciences, 81*(5), 467–470.
Sharma, S., & Tiwari, S. (2020). A review on biomacromolecular hydrogel classification and its applications. *International Journal of Biological Macromolecules, 162*, 737–747.
Shpaisman, N., Sheitet, L., Bushman, J., Winters, J., & Kohn, J. (2012). One-step synthesis of biodegradable curcumin-derived hydrogels as potential soft tissue fillers after breast cancer surgery. *Biomacromolecules, 13*, 2279–2286.
Sivakumaran, D., Maitland, D., Oszustowicz, T., & Hoare, T. (2013). Tuning drug release from smart microgel-hydrogel composites via cross-linking. *Journal of Colloid and Interface Science, 392*, 422–430.
Soleimani, K., Derakhshankhah, H., Jaymand, M., & Samadian, H. (2021). Stimuli-responsive natural gums-based drug delivery systems for cancer treatment. *Carbohydrate Polymers, 254*, Article 117422.
Srivastava, N., Kay, R. R., & Kabla, A. J. (2017). Method to study cell migration under uniaxial compression. *Molecular Biology of the Cell, 28*, 809–817.
Sung, H., Ferlay, J., Siegel, R. L., Laversanne, M., Soerjomataram, I., Jemal, A., & Bray, F. (2021). Global cancer statistics: GLOBOCAN estimates of incidence and mortality worldwide for 36 cancers in 185 countries. *CA: A Cancer Journal for Clinicians, 7*(3), 209–249.
Tang, R.-Z., Liu, Z.-Z., Gu, S.-S., & Liu, X.-Q. (2021). Multiple local therapeutics based on nano-hydrogel composites in breast cancer treatment. *Journal of Material Chemistry B, 9*, 1521.
Tian, B., Hua, S., & Liu, J. (2020). Cyclodextrin-based delivery systems for chemotherapeutic anticancer drugs: A review. *Carbohydrate Polymers, 232*, Article 115805.
Vigata, M., Meinert, C., Hutmacher, D. W., & Bock, N. (2020). Hydrogels as drug delivery systems: A review of current characterization and evalutation techniques. *Pharmaceutics, 12*(12), 1188.
Villareal-Otalvaro, C., & Coburn, M. (2021). Fabrication methods and form factors of gellan gum-based materials for drug delivery and anti-cancer applications. *ACS Biomater Sci. Eng.* In press.
Vu, T. T., Gulfam, M., Jo, S.-H., Park, S.-H., & Lim, K. T. (2022). Injectable and biocompatible alginate-derived porous hydrogels cross-linked by IEDDA click

chemistry for reduction-responsive drug release application. *Carbohydrate Polymers, 278*, Article 118964.
Výborný, K., Vallová, J., Kočí, Z., Kekulová, K., Jiráková, K., Jendelová, P., Hodan, J., & Kubinová, Š. (2019). Genipin and EDC crosslinking of extracellular matrix hydrogel derived from human umbilical cord for neural tissue repair. *Scientific Reports, 9*, 10674.
Wu, S.-W., Liu, X., Miller, A. L., II, Cheng, Y.-S., Yeh, M.-L., & Lu, L. (2018). Strengthening injectable thermo-sensitive NIPAAm-g-chitosan hydrogels using chemical crosslinking of disulfide bonds as scaffolds for tissue engineering. *Carbohydrate Polymers, 192*, 308–316.
Xu, Z., Li, Z., Jiang, S., & Bratlie, K. M. (2018). Chemically modified gellan gum hydrogels with tunable properties for use as tissue engineering scaffolds. *ACS Omega, 3*, 6998–7007.
Xu, K., Yao, H., Fan, D., Zhou, L., & Wei, S. (2021). Hyaluronic acid thiol modified injectable hydrogel: Synthesis, characterization, drug release, cellular drug uptake and anticancer activity. *Carbohydrate Polymers, 254*, Article 117286.
Yu, Y., Zhu, S., Wu, D., Li, L., Zhou, C., & Lu, L. (2020). Thiolated gellan gum hydrogels as a peptide delivery system for 3D neural stem cell culture. *Materials Letters, 259*, Article 126891.
Zhou, Y., & Jin, L. (2020). Hydrolysis-induced large swelling of polyacrylamide hydrogels. *Soft Matter Journal, 16*, 5740.
Zhuang, B., Chen, T., Xiao, Z., & Jin, Y. (2020). Drug-loaded implantable surgical cavity-adaptative hydrogels for prevention of local tumor recurrence. *International Journal of Pharmaceutics, 577*, Article 119048.